IEEE Access
Multidisciplinary | Rapid Review | Open Access Journal

Received May 30, 2019, accepted June 26, 2019, date of publication July 1, 2019, date of current version August 1, 2019.

Digital Object Identifier 10.1109/ACCESS.2019.2925962

Analysis of Electromagnetic Scattering From Combined Conducting and Dielectric Objects Above Rough Surface Using Hybrid SIE-KA-FMM Method

GAOXIANG ZOU[1], CHUANGMING TONG[1], HUALONG SUN[1], PENG PENG[1,2], AND TAO SONG[1]

[1]Air and Missile Defense College, Air Force Engineering University, Xi'an 710051, China
[2]School of Physics and Optoelectronic Engineering, Xidian University, Xi'an 710126, China

Corresponding author: Gaoxiang Zou (gxiangzou@163.com)

This work was supported by the National Natural Science Foundation of China under Grant 61372033.

ABSTRACT An efficient hybrid SIE-KA-FMM method is presented to analyze the electromagnetic scattering from combined conducting and dielectric objects above the rough surface. In this approach, the induced electric current on the rough surface is obtained by the Kirchhoff approximation (KA). The single integral equation (SIE) method is utilized to efficiently compute scattering from the composite target with markedly reducing the numbers of unknowns compared with the conventional coupled integral equation method. The fast multi-pole method (FMM) is incorporated for faster operation and less memory requirement. Several examples verify the validation of the hybrid SIE-KA-FMM method. The composite scattering characteristics of diversiform targets above the rough surface are obtained. Moreover, the numerical results with the different permittivity of dielectric part, polarization mode, working frequency, root mean square (RMS) and correlation length of rough surface, incident pitching/azimuth angle, and target height and target category have been analyzed to provide some useful conclusions.

INDEX TERMS Kirchhoff approximation, single integral equation, fast multi-pole method, combined conductor and dielectric objects, rough surface, composite scattering.

I. INTRODUCTION

In recent years, the characteristics of electromagnetic scattering from three-dimensional objects with complex geometrical structure or composite material have been widely studied [1]–[6] due to its wide application prospects in both civil and military field. Typical calculation methods have been proposed to solve the scattering from object, including finite-difference time-domain (FDTD) method [7], [8], finite element method (FEM) [9], [10] and method of moment (MOM) [11], [12]. Many relevant applications for solving scattering from perfect electrical conductor (PEC) target have been proposed, which verify the efficiency of numerical algorithm. Most of these methods could be applied to analyze more complicated target such as combined conducting and dielectric object, but their performance in accuracy and efficiency aspects would be restricted by various factors. Several attempts have been made to deal with the scattering problems of combined conducting and dielectric objects. For instance, FEM is the core algorithm in commercial software High Frequency Simulator Structure (HFSS), which has strong adaptability to most of scattering problem, but huge unknowns will be created when analyzing three-dimensional electrically large composite object. FDTD method has the same weakness when solving this kind of problem. Previous researches have shown that integral equation method could solve this problem efficiently, including surface integral equation method [13] and volume integral equation method [14]. Volume integral equation method is very suitable for calculating the scattering of inhomogeneous dielectric material, but due to its volumetric dissection pattern, the number of unknowns will seriously increase with the increase of electrical size or dielectric constant. In the past decades, several acceleration strategies have been proposed to improve this method, which can be generally classified into two categories: The first category is accelerating the process of matrix equations by virtue of mathematical operations, e.g., fast multi-pole method (FMM) [15] and multi-level fast multi-pole

The associate editor coordinating the review of this manuscript and approving it for publication was Zhengqing Yun.

method (MLFMM) [16]. The second category is utilized high order basic functions to discretize vector integral equations aiming at obtaining a much compressed linear scalar matrix equation. This kind of method can greatly decrease the number of unknowns in the final matrix equations, e.g., characteristic basis function method (CBFM) [17] and synthetic functions expansion (SFX) [18]–[20]. Even if introducing some acceleration strategies above, its calculation efficiency and capability will be severely restricted. However, in general, actual dielectric materials are always homogeneous or segmented uniform. Hence, we choose surface integral equation method and we can analyze the scattering characteristics of dielectric material more efficiently. The basic operation of surface integral equation method is divided into two parts: firstly, formulating electric field integral equation (EFIE), magnetic field integral equation (MFIE) or combined field integral equation (CFIE) for conducting region; secondly, formulating Poggio-Miller-Chang-Harrington-Wu-Tsai (PMCHWT) equations [21]–[23] for dielectric region. Therefore, the equivalent electric current and equivalent magnetic current have to be calculated. In Ref. [24], instead of using general integral equation, the single integral equation (SIE) method is firstly utilized to solve the scattering problem of dielectric bodies, because only single effective current needs to be calculated and half of unknowns could be cut down. In Ref. [25] and Ref. [26], these studies provide fresh insights into solving scattering from combined conducting and dielectric object using SIE method.

Such approach has only focus on the scattering characteristics of target. However, in actual target detection process, the background environment is also an important factor to effect on the total scattering field. Recently, researchers have shown an increased interest in studying the composite scattering characteristics owning to its wide applications such as radar detection, remote sensing and SAR imaging [27]–[29]. When the background environment is considered, numerical methods have to deal with huge number of unknowns. Previous researches have shown that the hybrid method of numerical algorithm and high frequency approximation algorithm could have a great performance in solve the composite scattering problems, such as KA-MOM [30], PO-MM [31], combined KA with the hybrid finite element-boundary integral method (FE-BI-KA) [32]. Among them, the hybrid KA-MOM method is the most representative and widely applied, which provides an efficient way to model the interaction between target and underlying environment. The hybrid KA-MOM method has less time consumption and smaller memory occupancy than traditional MOM. Previously published studies have tended to focus on single target rather than composite target. However, actual target always has both conducting part and dielectric part. Therefore, we choose this kind of algorithm framework, combined with the SIE method mentioned before, to make some attempts of analyzing scattering from combined conducting and dielectric objects above rough surface. Meanwhile, efficient acceleration strategy is introduced to speed up calculating processes.

This paper is organized as follow: In Section II, the theoretical formulations of hybrid SIE-KA method are derived in detail. The fast multi-pole method (FMM) is introduced to accelerate the calculation processes and corresponding operation processes are given. Several examples verify the validation of the hybrid SIE-KA-FMM method. In Section III, the differences of electromagnetic scattering from PEC target, dielectric target and composite target above rough surface are compared. The influences of permittivity of dielectric part, polarization mode, working frequency, root mean square (RMS) and correlation length of rough surface, incident pitching or azimuth angle, target height and target category on scattering characteristic are discussed in detail. In Section IV, a summary of this new method is made and a proposition for further investigation is given.

II. FORMULATION

A. HYBRID SIE-KA METHOD

The geometrical models of target and environment are disserted by triangulation. N_1 denotes the total number of edges in PEC region S_1 of target, which contains the common edges in the contacting boundary between PEC region S_1 and dielectric region S_2. N_2 denotes the total number of edges in dielectric region S_2 of target, and it doesn't contain the common edge. The contacting surface between PEC region and dielectric region is surface S_3. N_3 denotes the total number of edges in contacting surface S_3. The inner surface of dielectric region of target is defined as surface $S_d = S_2 + S_3$. Gauss spectrum [33] is widely used to model ground rough surface, whose statistic property is determined by RMS height h_{rms} and correlation length l_x and l_y in x and y direction. The rough surface model is established based on the Gauss spectrum. N_4 denotes the total number of edges in Gauss rough surface S_4.

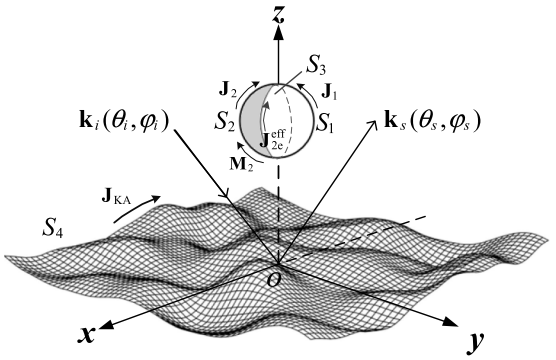

FIGURE 1. Illustration of the composite target above rough surface.

As shown in Figure 1, when electromagnetic wave illuminates target or rough surface, the equivalent electric/magnetic current will be stimulated on the surface in different region. $\mathbf{J}_1$ denotes the equivalent electric current on the PEC region S_1 of target. $\mathbf{J}_2$ and $\mathbf{M}_2$ denote the equivalent electric and magnetic current respectively on the dielectric region S_2 of target. Assume the Gauss rough surface as PEC surface. $\mathbf{J}_{KA}$ denotes the equivalent electric current on Gauss rough surface

S_4. $\mathbf{J}_1$, bf J_2, $\mathbf{M}_2$ and $\mathbf{J}_{\mathrm{KA}}$ can be expanded by RWG basis functions [11]:

$$\text{PEC region } S_1 \ \eta_0\mathbf{J}_1 = \sum_{j=1}^{N_1} a_j\mathbf{f}_{1j} \tag{1}$$

$$\text{Dielectric region } S_2 \begin{cases} \eta_0\mathbf{J}_2 = \sum_{j=1}^{N_2} b_j\mathbf{f}_{2j} \\ \mathbf{M}_2 = \sum_{j=1}^{N_2} c_j\mathbf{f}_{2j} \end{cases} \tag{2}$$

$$\text{Environmental surface } S_4 \ \eta_0\mathbf{J}_{\mathrm{KA}} = \sum_{j=1}^{N_4} d_j\mathbf{f}_{4j} \tag{3}$$

According to Ref. [24], effective electric current $\mathbf{J}_{2\mathrm{e}}^{\mathrm{eff}}$ will be stimulated on the inner surface S_{d}. The effective electric current $\mathbf{J}_{2\mathrm{e}}^{\mathrm{eff}}$ be expanded by the RWG basis functions:

$$\text{Inner surface } S_{\mathrm{d}} - \eta_0\mathbf{J}_{2\mathrm{e}}^{\mathrm{eff}} = \sum_{j=1}^{N_2} g_j\mathbf{f}_{2j} + \sum_{j=1}^{N_3} h_j\mathbf{f}_{3j} \tag{4}$$

In which, $\mathbf{f}_{1j}$, $\mathbf{f}_{2j}$, $\mathbf{f}_{3j}$ and $\mathbf{f}_{4j}$ are RWG basis function. a_j denotes the expansion coefficient of $\mathbf{J}_1$ on the PEC region S_1 of target. b_j and c_j denote the expansion coefficient of $\mathbf{J}_2$ and $\mathbf{M}_2$ on the dielectric region S_2 of target respectively. d_j denotes the expansion coefficient of $\mathbf{J}_{\mathrm{KA}}$ on Gauss rough surface. According to the Huyghens' equivalence principle, induced electric current $\mathbf{J}_{\mathrm{KA}}$ on rough surface can be written as $\mathbf{J}_{\mathrm{KA}} = \hat{\mathbf{n}}_4 \times \mathbf{H}_{\mathrm{sur}}$, where $\hat{\mathbf{n}}_4$ denotes the unit normal vector of arbitrary point of rough surface and $\mathbf{H}_{\mathrm{sur}}$ presents the total magnetic field. When there is no target above the rough surface, total magnetic field $\mathbf{H}_{\mathrm{sur}}$ is determined by the incident magnetic field $\mathbf{H}^{\mathrm{i}}$ and scattering magnetic field $\mathbf{H}_{\mathrm{sur}}^{\mathrm{s}}$. If there is a target above rough surface, the influence of mutual coupling between them must be taken into consideration. Meanwhile, the total magnetic field of rough surface can be written as follow:

$$\mathbf{H}_{\mathrm{sur}} = \mathbf{H}^{\mathrm{i}} + \mathbf{H}_{\mathrm{sur}}^{\mathrm{s}} + \mathbf{H}_{\mathrm{t\text{-}sur}}^{\mathrm{s}} \tag{5}$$

In which,$\mathbf{H}_{\mathrm{t\text{-}sur}}^{\mathrm{s}}$ presents the incident magnetic field from the secondary incidence resource: combined conducting and dielectric target. Its expression is written as follow:

$$\mathbf{H}_{\mathrm{t\text{-}sur}}^{\mathrm{s}} = -\mathbf{K}_{01}(\mathbf{J}_1) - \frac{1}{\eta_0}\mathbf{L}_{02}(\mathbf{M}_2) - \mathbf{K}_{02}(\mathbf{J}_2) \tag{6}$$

Here η_0 is the characteristic impedance in free space. $\mathbf{L}_{0z}(\cdot)$ and $\mathbf{K}_{0z}(\cdot)$ present electric field integral operator (EFIO) and magnetic field integral operator (MFIO) respectively, which are taken in the form:

$$\mathbf{L}_{0z}(\mathbf{X}) = jk_0\int_{S_z}\left[G_0(\mathbf{r},\mathbf{r}')\mathbf{X}(\mathbf{r}') + \frac{1}{k_0^2}\nabla G_0(\mathbf{r},\mathbf{r}')\nabla'\cdot\mathbf{X}(\mathbf{r}')\right]dS' \quad z = 1, 2 \text{ or } 4 \tag{7a}$$

$$\mathbf{K}_{0z}(\mathbf{X}) = \int_{S_z}\left[\mathbf{X}(\mathbf{r}')\times\nabla G_0(\mathbf{r},\mathbf{r}')\right]dS' \quad z = 1, 2 \text{ or } 4 \tag{7b}$$

where $G_0(\mathbf{r},\mathbf{r}')$ is the Green function in free space, and its expression is $G_0(\mathbf{r},\mathbf{r}') = e^{-jk|\mathbf{r}-\mathbf{r}'|}/(4\pi\left|\mathbf{r}-\mathbf{r}'\right|)$. When radius of curvature ρ of every point on the rough surface and incident wavelength λ meet the relationship:$\rho >> \lambda$, this rough surface meets the Kirchhoff approximation condition. The Equation of $\mathbf{H}_{\mathrm{sur}}^{\mathrm{s}}$ is taken in the form:

$$\mathbf{H}_{\mathrm{sur}}^{\mathrm{s}} = \frac{1}{\eta_0}\hat{\mathbf{k}}_{\mathrm{r}}\times(\Gamma_{\parallel}\mathrm{E}_{\parallel}^{\mathrm{i}}\hat{\mathbf{e}}_{\mathrm{i}\parallel} + \Gamma_{\perp}\mathrm{E}_{\perp}^{\mathrm{i}}\hat{\mathbf{e}}_{\mathrm{i}\perp} + \Gamma_{\parallel}\mathrm{E}_{\mathrm{t\text{-}sur}\parallel}^{\mathrm{s}}\hat{\mathbf{e}}_{\mathrm{i}\parallel} + \Gamma_{\perp}\mathrm{E}_{\mathrm{t\text{-}sur}\perp}^{\mathrm{s}}\hat{\mathbf{e}}_{\mathrm{i}\perp}) \tag{8}$$

where the local reflection direction is presented as $\hat{\mathbf{k}}_{\mathrm{r}} = \hat{\mathbf{k}}_{\mathrm{i}} - 2\hat{\mathbf{n}}(\hat{\mathbf{n}}\cdot\hat{\mathbf{k}}_{\mathrm{i}})$; the local orthogonal system is $(\hat{\mathbf{e}}_{\mathrm{i}\parallel}, \hat{\mathbf{e}}_{\mathrm{i}\perp}, \hat{\mathbf{k}}_{\mathrm{i}})$; the vector of horizontal/vertical polarization can be presented as: $\hat{\mathbf{e}}_{\mathrm{i}\parallel} = \left(\hat{\mathbf{n}}\times\hat{\mathbf{k}}_{\mathrm{i}}\right)\Big/\left|\hat{\mathbf{n}}\times\hat{\mathbf{k}}_{\mathrm{i}}\right|$, $\hat{\mathbf{e}}_{\mathrm{i}\perp} = \hat{\mathbf{e}}_{\mathrm{i}\parallel}\times\hat{\mathbf{k}}_{\mathrm{i}}$; the local incident angle is determined by expression $\cos\theta' = -\hat{\mathbf{n}}\cdot\hat{\mathbf{k}}_{\mathrm{i}}$; $\Gamma_{\parallel}$ and $\Gamma_{\perp}$ are horizontal and vertical polarization component of Fresnel reflection coefficient, which is taken in this form:

$$\Gamma_{\parallel} = \frac{\cos\theta' - \sqrt{\varepsilon_{\mathrm{r}}\mu_{\mathrm{r}} - \sin^2\theta'}}{\cos\theta' + \sqrt{\varepsilon_{\mathrm{r}}\mu_{\mathrm{r}} - \sin^2\theta'}} \tag{9a}$$

$$\Gamma_{\perp} = \frac{\varepsilon_{\mathrm{r}}\cos\theta' - \sqrt{\varepsilon_{\mathrm{r}}\mu_{\mathrm{r}} - \sin^2\theta'}}{\varepsilon_{\mathrm{r}}\cos\theta' + \sqrt{\varepsilon_{\mathrm{r}}\mu_{\mathrm{r}} - \sin^2\theta'}} \tag{9b}$$

Considering the influence of secondary incidence resource by target, incident magnetic field can be presented as

$$\mathbf{H}^{i} = \frac{1}{\eta_0}\hat{\mathbf{k}}_{i}\times(\mathrm{E}_{\parallel}^{\mathrm{i}}\hat{\mathbf{e}}_{\mathrm{i}\parallel} + \mathrm{E}_{\perp}^{\mathrm{i}}\hat{\mathbf{e}}_{\mathrm{i}\perp} + \mathrm{E}_{\mathrm{t\text{-}sur}\parallel}^{\mathrm{s}}\hat{\mathbf{e}}_{\mathrm{i}\parallel} + \mathrm{E}_{\mathrm{t\text{-}sur}\perp}^{\mathrm{s}}\hat{\mathbf{e}}_{\mathrm{i}\perp}) \tag{10}$$

Substitute (8) and (10) into (40), the expression of (40) can be transformed as follow:

$$\begin{aligned}\mathbf{H}_{\mathrm{sur}} = {} & \frac{1}{\eta_0}\hat{\mathbf{k}}_{\mathrm{i}}\times(\mathrm{E}_{\parallel}^{\mathrm{i}}\hat{\mathbf{e}}_{\mathrm{i}\parallel} + \mathrm{E}_{\perp}^{\mathrm{i}}\hat{\mathbf{e}}_{\mathrm{i}\perp} + \mathrm{E}_{\mathrm{t\text{-}sur}\parallel}^{\mathrm{s}}\hat{\mathbf{e}}_{\mathrm{i}\parallel} + \mathrm{E}_{\mathrm{t\text{-}sur}\perp}^{\mathrm{s}}\hat{\mathbf{e}}_{\mathrm{i}\perp}) \\ & + \frac{1}{\eta_0}\hat{\mathbf{k}}_{\mathrm{r}}\times(\Gamma_{\parallel}\mathrm{E}_{\parallel}^{\mathrm{i}}\hat{\mathbf{e}}_{\mathrm{i}\parallel} + \Gamma_{\perp}\mathrm{E}_{\perp}^{\mathrm{i}}\hat{\mathbf{e}}_{\mathrm{i}\perp} + \Gamma_{\parallel}\mathrm{E}_{\mathrm{t\text{-}sur}\parallel}^{\mathrm{s}}\hat{\mathbf{e}}_{\mathrm{i}\parallel} \\ & + \Gamma_{\perp}\mathrm{E}_{\mathrm{t\text{-}sur}\perp}^{\mathrm{s}}\hat{\mathbf{e}}_{\mathrm{i}\perp})\end{aligned} \tag{11}$$

Based on (11), the expression of $\mathbf{J}_{\mathrm{KA}}$ can be transformed as follow:

$$\begin{aligned}\mathbf{J}_{\mathrm{KA}} = {} & \frac{1}{\eta_0}\hat{\mathbf{n}}_4\times\left\{\hat{\mathbf{k}}_{\mathrm{i}}\times\left[(\mathbf{E}^{\mathrm{i}} + \mathbf{E}_{\mathrm{t\text{-}sur}}^{\mathrm{s}})\cdot\bar{\bar{\mathbf{e}}}_{\mathrm{i}\parallel} + (\mathbf{E}^{\mathrm{i}} + \mathbf{E}_{\mathrm{t\text{-}sur}}^{\mathrm{s}})\cdot\bar{\bar{\mathbf{e}}}_{\mathrm{i}\perp}\right]\right. \\ & \left. + \hat{\mathbf{k}}_{\mathrm{r}}\times\left[\Gamma_{\parallel}(\mathbf{E}^{\mathrm{i}} + \mathbf{E}_{\mathrm{t\text{-}sur}}^{\mathrm{s}})\cdot\bar{\bar{\mathbf{e}}}_{\mathrm{i}\parallel} + \Gamma_{\perp}(\mathbf{E}^{\mathrm{i}} + \mathbf{E}_{\mathrm{t\text{-}sur}}^{\mathrm{s}})\cdot\bar{\bar{\mathbf{e}}}_{\mathrm{i}\perp}\right]\right\}\end{aligned} \tag{12}$$

where $\bar{\bar{\mathbf{e}}}_{\mathrm{i}\parallel}$ and $\bar{\bar{\mathbf{e}}}_{\mathrm{i}\perp}$ present the dyadic of horizontal/vertical polarization: $\bar{\bar{\mathbf{e}}}_{\mathrm{i}\parallel} = \hat{\mathbf{e}}_{\mathrm{i}\parallel}\hat{\mathbf{e}}_{\mathrm{i}\parallel}$, $\bar{\bar{\mathbf{e}}}_{\mathrm{i}\perp} = \hat{\mathbf{e}}_{\mathrm{i}\perp}\hat{\mathbf{e}}_{\mathrm{i}\perp}$. Substitute (1)-(3) and (6) into (12), then both sides of (12) are tested by $\hat{\mathbf{n}}_4\times\mathbf{f}_{4i}$, the expression of (12) can be written in vector matrix form as follow:

$$\{d\} = [\mathrm{D}_{41}]\cdot\{a\} + [\mathrm{D}_{42}]\cdot\{b\} + [\mathrm{F}_{42}]\cdot\{c\} + \{\mathrm{W}\} \tag{13}$$

where the expressions of matrix elements are taken in these forms:

$$\mathrm{D}_{4q}(i,j) = -\int_{T_{4i}}\mathbf{f}_{4i}(\mathbf{r})\cdot[\hat{\mathbf{k}}_{\mathrm{i}}\times\left(\mathbf{L}_{0q}(\mathbf{f}_{qj})\cdot\bar{\bar{\mathbf{e}}}_{\mathrm{i}\parallel} + \mathbf{L}_{0q}(\mathbf{f}_{qj})\cdot\bar{\bar{\mathbf{e}}}_{\mathrm{i}\perp}\right)$$

$$+\hat{\mathbf{k}}_{\mathrm{r}} \times \left(\Gamma_{\parallel}\mathbf{L}_{0q}(\mathbf{f}_{qj})\cdot\bar{\bar{\mathbf{e}}}_{\mathrm{i}\parallel} + \Gamma_{\perp}\mathbf{L}_{0q}(\mathbf{f}_{qj})\cdot\bar{\bar{\mathbf{e}}}_{\mathrm{i}\perp}\right)\Big] dS, \quad i \in [1, N_4],\ j \in [1, N_q],\ q = 1, 2. \tag{14a}$$

$$\mathrm{F}_{42}(i,j) = \int_{T_{4i}} \mathbf{f}_{4i}(\mathbf{r})\cdot\Big[\hat{\mathbf{k}}_{\mathrm{i}} \times \left(\mathbf{K}_{02}(\mathbf{f}_{2j})\cdot\bar{\bar{\mathbf{e}}}_{\mathrm{i}\parallel} + \mathbf{K}_{02}(\mathbf{f}_{2j})\cdot\bar{\bar{\mathbf{e}}}_{\mathrm{i}\perp}\right) + \hat{\mathbf{k}}_{r} \times \left(\Gamma_{\parallel}\mathbf{K}_{02}(\mathbf{f}_{2j})\cdot\bar{\bar{\mathbf{e}}}_{\mathrm{i}\parallel} + \Gamma_{\perp}\mathbf{K}_{02}(\mathbf{f}_{2j})\cdot\bar{\bar{\mathbf{e}}}_{\mathrm{i}\perp}\right)\Big] dS, \quad i \in [1, N_4],\ j \in [1, N_2] \tag{14b}$$

$$\mathrm{W}(i) = \int_{T_{4i}} \mathbf{f}_{4i}(\mathbf{r})\cdot\Big[\hat{\mathbf{k}}_{\mathrm{i}} \times \left(\mathbf{E}^{\mathrm{i}}(\mathbf{r})\cdot\bar{\bar{\mathbf{e}}}_{\mathrm{i}\parallel} + \mathbf{E}^{\mathrm{i}}(\mathbf{r})\cdot\bar{\bar{\mathbf{e}}}_{\mathrm{i}\perp}\right) + \hat{\mathbf{k}}_{\mathrm{r}} \times \left(\Gamma_{\parallel}\mathbf{E}^{\mathrm{i}}(\mathbf{r})\cdot\bar{\bar{\mathbf{e}}}_{\mathrm{i}\parallel} + \Gamma_{\perp}\mathbf{E}^{\mathrm{i}}(\mathbf{r})\cdot\bar{\bar{\mathbf{e}}}_{\mathrm{i}\perp}\right)\Big] dS, \quad i \in [1, N_4] \tag{14c}$$

The expression of integral equation in PEC region S_1 of target is taken in this form:

$$\hat{\mathbf{n}}_1 \times \mathbf{E}^{\mathrm{s}}_{\mathrm{t}} = -\hat{\mathbf{n}}_1 \times (\mathbf{E}^{\mathrm{i}} + \mathbf{E}^{\mathrm{s}}_{\text{sur-t}})\mathbf{r} \in S_1 \tag{15a}$$

The expression of integral equation in dielectric region S_2 of target is taken in this form:

$$\hat{\mathbf{n}}_2 \times \mathbf{E}^{\mathrm{s}}_{\mathrm{t}} = -\hat{\mathbf{n}}_2 \times (\mathbf{E}^{\mathrm{i}} + \mathbf{E}^{\mathrm{s}}_{\text{sur-t}})\mathbf{r} \in S_2 \tag{15b}$$

where $\mathbf{E}^{\mathrm{s}}_{\mathrm{t}}$ presents the scattering electric field of target, which have the expression as follow:

$$\mathbf{E}^{\mathrm{s}}_{\mathrm{t}} = -\eta_0\mathbf{L}_{01}(\mathbf{J}_1) - \eta_0\mathbf{L}_{02}(\mathbf{J}_2) + \mathbf{K}_{02}(\mathbf{M}_2) \tag{16}$$

When the incident wave illuminates the PEC rough surface, induced electric current $\mathbf{E}^{\mathrm{s}}_{\text{sur-t}}$ is stimulated on the surface which will illuminate the target as the secondary incidence resource.

$$\mathbf{E}^{\mathrm{s}}_{\text{sur-t}} = -\eta_0\mathbf{L}_{04}(\mathbf{J}_{\mathrm{KA}}) \tag{17}$$

Substitute (16) and (17) into (15a) and (15b), the expression of (15a) and (15b) can be written as follow:

$$\hat{\mathbf{n}}_1 \times \mathbf{E}^{\mathrm{i}} = \hat{\mathbf{n}}_1 \times \Big[\mathbf{L}_{01}(\eta_0\mathbf{J}_1) + \mathbf{L}_{02}(\eta_0\mathbf{J}_2) - \tilde{\mathbf{K}}_{02}(\mathbf{M}_2) + \mathbf{L}_{04}(\eta_0\mathbf{J}_{\mathrm{KA}})\Big] \tag{18a}$$

$$\hat{\mathbf{n}}_2 \times \mathbf{E}^{\mathrm{i}} = \hat{\mathbf{n}}_2 \times \Big[\mathbf{L}_{01}(\eta_0\mathbf{J}_1) + \mathbf{L}_{02}(\eta_0\mathbf{J}_2) - (1/2)\mathbf{M}_2 - \tilde{\mathbf{K}}_{02}(\mathbf{M}_2) + \mathbf{L}_{04}(\eta_0\mathbf{J}_{\mathrm{KA}})\Big] \tag{18b}$$

Substitute (1)-(3) into (18a) and (18b), then, both sides of (18a) are tested by $\hat{\mathbf{n}}_1 \times \mathbf{f}_{1i}$, both sides of (18b) are tested by $\hat{\mathbf{n}}_2 \times \mathbf{f}_{2i}$, the expression of (18a) and (18b) can be written in vector matrix form as follow:

$$\left[\mathrm{Q}_{11}\right]\cdot\{a\} + \left[\mathrm{Q}_{12}\right]\cdot\{b\} + [\mathrm{P}_{12}]\cdot\{c\} + [\mathrm{R}_{14}]\cdot\{d\} = \{\mathrm{S}_1\} \tag{19a}$$

$$\left[\mathrm{Q}_{21}\right]\cdot\{a\} + \left[\mathrm{Q}_{22}\right]\cdot\{b\} + [\mathrm{P}_{22}]\cdot\{c\} + [\mathrm{R}_{24}]\cdot\{d\} = \{\mathrm{S}_2\} \tag{19b}$$

where the expressions of matrix elements are taken in these forms:

$$\mathrm{Q}_{pq}(i,j) = \int_{T_{pi}} \mathbf{f}_{pi}(\mathbf{r})\cdot\mathbf{L}_{0q}(\mathbf{f}_{qj})dS, \quad i \in [1, N_p],\ j \in [1, N_q]\ p, q = 1, 2. \tag{20a}$$

$$\mathrm{P}_{12}(i,j) = -\int_{T_{1i}} \mathbf{f}_{1i}(\mathbf{r})\cdot\tilde{\mathbf{K}}_{02}(\mathbf{f}_{2j})dS, \quad i \in [1, N_1],\ j \in [1, N_2] \tag{20b}$$

$$\mathrm{P}_{22}(i,j) = -\frac{\delta_{ij}}{2} - \int_{T_{2i}} \mathbf{f}_{2i}(\mathbf{r})\cdot\tilde{\mathbf{K}}_{02}(\mathbf{f}_{2j})dS, \quad i,j \in [1, N_2] \tag{20c}$$

$$\mathrm{R}_{p4}(i,j) = \int_{T_{pi}} \mathbf{f}_{pi}(\mathbf{r})\cdot\mathbf{L}_{04}(\mathbf{f}_{4j})dS, \quad i \in [1, N_p],\ j \in [1, N_4]\ p = 1, 2. \tag{20d}$$

$$\mathrm{S}_p(i) = \int_{T_{pi}} \mathbf{f}_{pi}(\mathbf{r})\cdot\mathbf{E}^{i}(\mathbf{r})dS,\ i \in [1, N_p],\ p = 1, 2 \tag{20e}$$

In (20c), if $i = j$, $\delta_{ij} = 1$;if $i \neq j$, $\delta_{ij} = 0$. If we substitute (13) into (19a) and (19b), we just need to calculate $\{a\}$, $\{b\}$ and $\{c\}$. To solve for $\{a\}$, $\{b\}$ and $\{c\}$, we have to consider the fields within the dielectric region of target. Hence, the SIE method is introduced to solve this problem. The fields in the dielectric region are generated by the effective electric current, whose expression refers to (4). The effective electric current $\mathbf{J}^{\mathrm{eff}}_{2\mathrm{e}}$ on the inner surface S_{d} generates the electric field $\mathbf{E}_{\mathrm{d}}$ and magnetic field $\mathbf{H}_{\mathrm{d}}$, whose expressions are taken in this form:

$$\mathbf{E}_{\mathrm{d}} = -\eta_1\mathbf{L}_{1\mathrm{d}}(\mathbf{J}^{\mathrm{eff}}_{2\mathrm{e}}) \tag{21a}$$

$$\mathbf{H}_{\mathrm{d}} = -\mathbf{K}_{1\mathrm{d}}(\mathbf{J}^{\mathrm{eff}}_{2\mathrm{e}}) \tag{21b}$$

where η_1 denotes characteristic impedance, whose expression is $\eta_1 = \sqrt{\mu_1/\varepsilon_1}$; μ_1 and ε_1 present conductivity and permittivity respectively. The operator $\mathbf{L}_{1d}(\cdot)$ and $\mathbf{K}_{1d}(\cdot)$ are the same as by changing the medium parameters and the integration over the inner surface of dielectric region S_{d}. The relationship between induced electric current and induced magnetic current on surface S_2 and effective electric current $\mathbf{J}^{\mathrm{eff}}_{2\mathrm{e}}$ can be determined by the boundary conditions as follow:

$$\mathbf{J}_2 = \hat{\mathbf{n}}_2 \times \mathbf{H}_{\mathrm{d}} = -\frac{1}{2}\mathbf{J}^{\mathrm{eff}}_{2\mathrm{e}} - \hat{\mathbf{n}}_2 \times \tilde{\mathbf{K}}_{1\mathrm{d}}(\mathbf{J}^{\mathrm{eff}}_{2\mathrm{e}}) \tag{22a}$$

$$-\mathbf{M}_2 = \hat{\mathbf{n}}_2 \times \mathbf{E}_{\mathrm{d}} = -\hat{\mathbf{n}}_2 \times \eta_1\mathbf{L}_{1\mathrm{d}}(\mathbf{J}^{\mathrm{eff}}_{2\mathrm{e}}) \tag{22b}$$

The tangential electric field component on the contacting surface S_3 will vanish, and the relational expression between $\mathbf{E}_{\mathrm{d}}$ and $\mathbf{J}^{\mathrm{eff}}_{2\mathrm{e}}$ is taken in this form:

$$0 = \hat{\mathbf{n}}_3 \times \mathbf{E}_{\mathrm{d}} = -\hat{\mathbf{n}}_3 \times \eta_1\mathbf{L}_{1\mathrm{d}}(\mathbf{J}^{\mathrm{eff}}_{2\mathrm{e}}) \tag{22c}$$

The effective electric current $\mathbf{J}^{\mathrm{eff}}_{2\mathrm{e}}$ on the inner surface S_{d} can be expanded by RWG basis function as (4). The expansion coefficient g_j and h_j of equivalent current can be approximated by average value of edge electric current as follow:

$$g_j = \frac{1}{l_{2j}}\int_{l_{2j}} (\hat{l}_{2j} \times \hat{\mathbf{n}}_{2j})\cdot(-\eta_0\mathbf{J}^{\mathrm{eff}}_{2\mathrm{e}})dl \tag{23a}$$

$$h_j = \frac{1}{l_{3j}}\int_{l_{3j}} (\hat{l}_{3j} \times \hat{\mathbf{n}}_{3j})\cdot(-\eta_0\mathbf{J}^{\mathrm{eff}}_{2\mathrm{e}})dl \tag{23b}$$

Substitute (2) into (22a) and (22b), then, both sides of (22a) and (22b) are tested by $\hat{\mathbf{n}}_2 \times \mathbf{f}_{2i}$, both sides of (22c) are tested

by $\hat{\mathbf{n}}_3 \times \mathbf{f}_{3i}$, the expression of (22a)-(22c) can be written in vector matrix form as follow:

$$\{b\} = \left[\tilde{\mathrm{M}}_{22}\right] \cdot \{g\} + \left[\tilde{\mathrm{M}}_{23}\right] \cdot \{h\} \tag{24a}$$

$$\{c\} = \left[\tilde{\mathrm{N}}_{22}\right] \cdot \{g\} + \left[\tilde{\mathrm{N}}_{23}\right] \cdot \{h\} \tag{24b}$$

$$\{0\} = \left[\tilde{\mathrm{B}}_{32}\right] \cdot \{g\} + \left[\tilde{\mathrm{B}}_{33}\right] \cdot \{h\} \tag{24c}$$

where the expressions of matrix elements are taken in these forms:

$$\tilde{M}_{22}(i,j) = \frac{\delta_{ij}}{2} + \int_{l_{2i}} \frac{\hat{l}_{2i}}{l_{2i}} \cdot \tilde{\mathbf{K}}_{1\mathrm{d}}(\mathbf{f}_{2j}) dl, \quad i,\ j \in [1, N_2] \tag{25a}$$

$$\tilde{M}_{23}(i,j) = \int_{l_{2i}} \frac{\hat{l}_{2i}}{l_{2i}} \cdot \tilde{\mathbf{K}}_{1\mathrm{d}}(\mathbf{f}_{3j}) dl, \ i \in [1, N_2],\ j \in [1, N_3] \tag{25b}$$

$$\tilde{N}_{2q}(i,j) = \int_{l_{2i}} \frac{\hat{l}_{2i}}{l_{2i}} \cdot \frac{\eta_1}{\eta_0} \mathbf{L}_{1\mathrm{d}}(\mathbf{f}_{qj}) dl, \quad i \in [1, N_2],\ j \in [1, N_q] \quad q = 2, 3. \tag{25c}$$

$$\tilde{B}_{3q}(i,j) = \int_{T_{3i}} \mathbf{f}_{3i}(\mathbf{r}) \cdot \frac{\eta_1}{\eta_0} \mathbf{L}_{1\mathrm{d}}(\mathbf{f}_{qj}) dS, \quad i \in [1, N_3], \quad j \in [1, N_q]\ q = 2, 3. \tag{25d}$$

In (26a), if $i = j$, $\delta_{ij} = 1$;if $i \neq j$, $\delta_{ij} = 0$. Combined with (24a), (24b) and (24c), (19a) and (19b) can be written in matrix equation as follow:

$$\begin{bmatrix} \mathrm{A}_{11} & \mathrm{A}_{12} & \mathrm{A}_{13} \\ \mathrm{A}_{21} & \mathrm{A}_{22} & \mathrm{A}_{23} \\ 0 & \mathrm{A}_{32} & \mathrm{A}_{33} \end{bmatrix} \cdot \begin{Bmatrix} a \\ g \\ h \end{Bmatrix} = \begin{Bmatrix} \tilde{\mathrm{S}}_1 \\ \tilde{\mathrm{S}}_2 \\ 0 \end{Bmatrix} \tag{26}$$

where the expressions of matrix elements are taken in these forms:

$$[\mathrm{A}_{11}] = \left[\mathrm{Q}_{11}\right] + [\mathrm{R}_{14}] \cdot [\mathrm{D}_{41}] \tag{27a}$$

$$[\mathrm{A}_{12}] = \left(\left[\mathrm{Q}_{12}\right] + [\mathrm{R}_{14}] \cdot [\mathrm{D}_{42}]\right) \cdot \left[\tilde{\mathrm{M}}_{22}\right] + \left([\mathrm{P}_{12}] + [\mathrm{R}_{14}] \cdot [\mathrm{F}_{42}] \right) \cdot \left[\tilde{\mathrm{N}}_{22}\right] \tag{27b}$$

$$[\mathrm{A}_{13}] = \left(\left[\mathrm{Q}_{12}\right] + [\mathrm{R}_{14}] \cdot [\mathrm{D}_{42}]\right) \cdot \left[\tilde{\mathrm{M}}_{23}\right] + \left([\mathrm{P}_{12}] + [\mathrm{R}_{14}] \cdot [\mathrm{F}_{42}] \right) \cdot \left[\tilde{\mathrm{N}}_{23}\right] \tag{27c}$$

$$[\mathrm{A}_{21}] = \left[\mathrm{Q}_{21}\right] + [\mathrm{R}_{24}] \cdot [\mathrm{D}_{41}] \tag{27d}$$

$$[\mathrm{A}_{22}] = \left(\left[\mathrm{Q}_{22}\right] + [\mathrm{R}_{24}] \cdot [\mathrm{D}_{42}]\right) \cdot \left[\tilde{\mathrm{M}}_{22}\right] + \left([\mathrm{P}_{22}] + [\mathrm{R}_{24}] \cdot [\mathrm{F}_{42}] \right) \cdot \left[\tilde{\mathrm{N}}_{22}\right] \tag{27e}$$

$$[\mathrm{A}_{23}] = \left(\left[\mathrm{Q}_{22}\right] + [\mathrm{R}_{24}] \cdot [\mathrm{D}_{42}]\right) \cdot \left[\tilde{\mathrm{M}}_{23}\right] + \left([\mathrm{P}_{22}] + [\mathrm{R}_{24}] \cdot [\mathrm{F}_{42}] \right) \cdot \left[\tilde{\mathrm{N}}_{23}\right] \tag{27f}$$

$$[\mathrm{A}_{32}] = \left[\tilde{\mathrm{B}}_{32}\right] \tag{27g}$$

$$[\mathrm{A}_{33}] = \left[\tilde{\mathrm{B}}_{33}\right] \tag{27h}$$

$$\left[\tilde{\mathrm{S}}_1\right] = \{\mathrm{S}_1\} - [\mathrm{R}_{14}] \cdot \{\mathrm{W}\} \tag{27i}$$

$$\left[\tilde{\mathrm{S}}_2\right] = \{\mathrm{S}_2\} - [\mathrm{R}_{24}] \cdot \{\mathrm{W}\} \tag{27j}$$

B. ACCELERATION OF THE HYBRID SIE-KA METHOD USING FAST MULTIPOLE ALGORITHM

If we directly adopt the surface integral equation method to solve the composite scattering problem, the dimension of the impedance matrix depends on the number of total unknowns $N_1+N_2+N_3+N_4$, where $N_4 >> N_1+N_2+N_3$. By utilizing the hybrid SIE-KA method, the dimension of impedance matrix only depends on the number of target's unknowns $N_1 + N_2 + N_3$. To further accelerate the computing speed and reduce memory requirement of hybrid SIE-KA method, FMM is introduced to solve the equation (26) efficiently. The essence of FMM is expression of Green function, which is based on the vector addition theorem [16]:

$$\begin{aligned} G(\mathbf{r}_o, \mathbf{r}_{o'}) &= \frac{e^{-jk|\mathbf{r}_o - \mathbf{r}_{o'}|}}{4\pi\,|\mathbf{r}_o - \mathbf{r}_{o'}|} \\ &= \frac{-jk}{(4\pi)^2} \oint d^2\hat{\mathrm{k}} e^{-j\mathbf{k}\mathbf{r}_{om}} T(\hat{\mathrm{k}}, \hat{\mathbf{r}}_{mm'}) e^{j\mathbf{k}\mathbf{r}_{o'm'}} \end{aligned} \tag{28}$$

where

$$T(\hat{k}, \mathbf{r}_{mm'}) = \sum_{l=0}^{L} (-j)^l (2l+1) \mathrm{h}_l^{(2)}(k r_{mm'}) \mathrm{P}_l(\hat{\mathrm{k}} \cdot \hat{\mathbf{r}}_{mm'}) \tag{29}$$

Correspondingly, the dyadic expression of Green function can be written as follow:

$$\begin{aligned} \bar{\bar{G}}(\mathbf{r}_o, \mathbf{r}_{o'}) &= (\bar{\bar{\mathbf{I}}} - \frac{\nabla\nabla'}{k}) \frac{e^{-jk|\mathbf{r}_o - \mathbf{r}_{o'}|}}{4\pi\,|\mathbf{r}_o - \mathbf{r}_{o'}|} \\ &= \frac{-jk}{(4\pi)^2} \oint d^2\hat{\mathrm{k}} (\bar{\bar{\mathbf{I}}} - \hat{\mathrm{k}}\hat{\mathrm{k}}) e^{-j\mathbf{k}\mathbf{r}_{om}} T(\hat{\mathrm{k}}, \mathbf{r}_{mm'}) e^{j\mathbf{k}\mathbf{r}_{o'm'}} \end{aligned} \tag{30}$$

Here, $\mathbf{r}_o$ resides in cube m centered at $\mathbf{r}_m$, $\mathbf{r}_{o'}$ resides in cube m' centered at $\mathbf{r}_{m'}$, and their relationships are: $\mathbf{r}_{om} = \mathbf{r}_o - \mathbf{r}_{m00}$, $\mathbf{r}_{o'm'} = \mathbf{r}_{o'} - \mathbf{r}_{m'}$. $\mathrm{h}_l^{(2)}(\cdot)$ denotes the spherical Hankel function of the second kind; $\mathrm{P}_l(\cdot)$ denotes the Legendre polynomial of degree l; L is the number of multi-pole expansion terms, and it can ensure high precision when set as $L = kd + 2\ln(kd + \pi)$. According to the Green function expressed in FMM, the matrix elements for far-region groups in matrix (13) D_{41}, D_{42} and F_{42} can be written as:

$$\begin{aligned} \mathrm{D}_{4q}(i,j) = \int\int d^2\hat{\mathrm{k}} \Big[& U_{im}^{\mathrm{D}_{44}} \cdot T_{mm'}(\mathbf{k}_0, \mathbf{r}_{mm'}) V_{jm'}^{\mathrm{D}_{qq}} \\ & + M_{im}^{\mathrm{D}_{44}} \cdot T_{mm'}(\mathbf{k}_0, \mathbf{r}_{mm'}) N_{jm'}^{\mathrm{D}_{qq}} \Big], \quad q = 1, 2. \end{aligned} \tag{31a}$$

$$\begin{aligned} \mathrm{F}_{42}(i,j) = \int\int d^2\hat{\mathrm{k}} \Big[& U_{im}^{\mathrm{F}_{44}} \cdot T_{mm'}(\mathbf{k}_0, \mathbf{r}_{mm'}) V_{jm'}^{\mathrm{F}_{22}} \\ & + M_{im}^{\mathrm{F}_{44}} \cdot T_{mm'}(\mathbf{k}_0, \mathbf{r}_{mm'}) N_{jm'}^{\mathrm{F}_{22}} \Big] \end{aligned} \tag{31b}$$

The expressions of every element in (31a) and (31b) are given in appendix (1-6). Where $U_{im}^{(\cdot)}/M_{im}^{(\cdot)}$, $T_{mm'}(\cdot)$ and $V_{jm'}^{(\cdot)}/N_{jm'}^{(\cdot)}$ are the disaggregation, translation and aggregation matrices on the concrete level respectively. Apply FMM to the integral equation of target, the matrix elements for far-region groups in matrix (19a) and (19b) Q_{11}, Q_{12}, Q_{21}, Q_{22}, P_{12}, P_{22}, R_{14} and R_{24} can be written as:

$$\mathrm{Q}_{pq}(i,j) = \int\int d^2\hat{\mathrm{k}} U_{im}^{\mathrm{Q}_{pp}} \cdot T_{mm'}(\mathbf{k}_0, \mathbf{r}_{mm'}) V_{jm'}^{\mathrm{Q}_{qq}}, \quad p, q = 1, 2. \tag{32a}$$

$$\mathrm{P}_{12}(i,j) = \int\int d^2\hat{\mathrm{k}} U_{im}^{\mathrm{P}_{11}} \cdot T_{mm'}(\mathbf{k}_0, \mathbf{r}_{mm'}) V_{jm'}^{\mathrm{P}_{22}} \quad (32b)$$

$$\mathrm{P}_{22}(i,j) = -\frac{\delta_{ij}}{2} + \int\int d^2\hat{\mathrm{k}} U_{im}^{\mathrm{P}_{22}} \cdot T_{mm'}(\mathbf{k}_0, \mathbf{r}_{mm'}) V_{jm'}^{\mathrm{P}_{22}} \quad (32c)$$

$$\mathrm{R}_{p4}(i,j) = \int\int d^2\hat{\mathrm{k}} U_{im}^{\mathrm{R}_{pp}} \cdot T_{mm'}(\mathbf{k}_0, \mathbf{r}_{mm'}) V_{jm'}^{\mathrm{R}_{44}}, \quad p = 1, 2. \quad (32d)$$

The expressions of every element in (32a)-(32d) are given in appendix (7-12). Where $U_{im}^{(\cdot)}$, $T_{mm'}(\cdot)$ and $V_{jm'}^{(\cdot)}$ are the disaggregation, translation and aggregation matrices on the concrete level respectively. In terms of Green function in dielectric region, the specific implementation process of FMM has to change according to the electromagnetic parameters of dielectric region particularly. Hence, in SIE method, the matrix elements for far-region groups in matrix (25a), (25b) and (25c) $\tilde{M}_{22}$, $\tilde{M}_{23}$, $\tilde{N}_{22}$, $\tilde{N}_{23}$, $\tilde{B}_{32}$ and $\tilde{B}_{33}$ can be written as:

$$\tilde{M}_{22}(i,j) = \frac{\delta_{ij}}{2} + \int\int d^2\hat{\mathrm{k}} U_{im}^{\tilde{M}_{22}} \cdot T_{mm'}(\mathbf{k}_1, \mathbf{r}_{mm'}) V_{jm'}^{\tilde{M}_{22}} \quad (33a)$$

$$\tilde{M}_{23}(i,j) = \int\int d^2\hat{\mathrm{k}} U_{im}^{\tilde{M}_{22}} \cdot T_{mm'}(\mathbf{k}_1, \mathbf{r}_{mm'}) V_{jm'}^{\tilde{M}_{33}} \quad (33b)$$

$$\tilde{N}_{2q}(i,j) = \int\int d^2\hat{\mathrm{k}} U_{im}^{\tilde{N}_{22}} \cdot T_{mm'}(\mathbf{k}_1, \mathbf{r}_{mm'}) V_{jm'}^{\tilde{N}_{qq}}, \quad q = 2, 3. \quad (33c)$$

$$\tilde{B}_{3q}(i,j) = \int\int d^2\hat{\mathrm{k}} U_{im}^{\tilde{B}_{33}} \cdot T_{mm'}(\mathbf{k}_1, \mathbf{r}_{mm'}) V_{jm'}^{\tilde{B}_{qq}}, \quad q = 2, 3. \quad (33d)$$

The expressions of every element in (33a)-(33d) are given in appendix (13-18). Where $U_{im}^{(\cdot)}$, $T_{mm'}(\cdot)$ and $V_{jm'}^{(\cdot)}$ are the disaggregation, translation and aggregation matrices on the concrete level respectively. Based on the above theory and formulations, the hybrid SIE-KA method with FMM are formed to calculate electromagnetic scattering from three-dimensional arbitrarily shaped combined conducting and dielectric target above rough surface. The bi-conjugate gradient (Bi-CG) method [34] is utilized to solve the matrix equation (26) iteratively. When the relative error of unknown electric/magnetic current between the n-th step and (n-1)-th step is less than 10^{-4}, the iterative computation stops.

In section A, when we introduce the SIE method to reduce the number of unknowns, the matrix condition number of EFIE is also improved. The MFIO $\mathbf{K}(\cdot)$ is the Fredholm operator of second kind, which is a compact operator. By contrast, the EFIO $\mathbf{L}(\cdot)$ is the Fredholm operator of first kind, which is a non-compact operator. The matrix condition number deduced by compact operator is superior to that of non-compact operator [35-36]. The compact operator of EFIE will cause worse matrix condition number. However, by introducing the SIE method, the hybrid SIE-KA-FMM method contains dual operator $\mathbf{L}_0 \cdot \mathbf{L}_0$, $\mathbf{L}_0 \cdot \tilde{\mathbf{K}}_1$ and $\tilde{\mathbf{K}}_0 \cdot \mathbf{L}_1$. There are two important conclusions in [36]: first, the product of compact operator and non-compact operator is compact operator; second, the product of two non-compact operators is compact operator. Therefore, these dual operators in hybrid SIE-KA-FMM are compact operator, which will improve the matrix condition number in dielectric part and accelerate the convergence speed of iteration solution.

C. VERIFICATION OF HYBRID SIE-KA-FMM METHOD

Firstly, we consider a small computation example to validate the efficiency of FMM. We choose the conventional MOM with LU scheme as the reference algorithm. Working frequency is set as 1GHz; Size of environment is $L_x \times L_y$: $10\lambda \times 10\lambda$; Gauss rough surface is PEC surface; Here, statistic parameters of Gauss rough surface are: $h_{\mathrm{rms}} = 0.1\lambda$ and $l_{\mathrm{x}} = l_{\mathrm{y}} = 2.0\lambda$; The radius of PEC sphere is 0.8λ; The height of sphere above the rough surface is 2.0λ. In this paper, a tapered incident beam is introduced in order to circumvent artificial truncation effects [37], and the 3-D form of it [38] is given as follow

$$E^{inc} = G(x,y,z) \cdot \exp[-jk_0(\cos\theta_i z - x\sin\theta_i\cos\varphi_i - y\sin\theta_i\sin\varphi_i)] \quad (34)$$

where

$$G(x,y,z) = \exp[-jk_0(\cos\theta_i z - x\sin\theta_i\cos\varphi_i - y\sin\theta_i\sin\varphi_i)w(x,y,z)]\exp(-t_x - t_y) \quad (35a)$$

$$t_x = (\cos\theta_i\cos\varphi_i x + \cos\theta_i\sin\varphi_i y + \sin\theta_i z)^2 / (g_x^2\cos^2\theta_i) \quad (35b)$$

$$t_y = (-\sin\varphi_i x + \cos\varphi_i y)^2 / g_y^2 \quad (35c)$$

$$w(x,y,z) = \left[(2t_x - 1)/(g_x^2\cos^2\theta_i) + (2t_y - 1)/g_y^2\right]/k_0^2 \quad (35d)$$

where the factors of beam width in x and y direction are set as $g_x = L_x/4$, $g_y = L_y/4$ in this paper. The incident angles are set as $\theta_i = 45°$ and $\varphi_i = 0°$. The observation angle ranges from $\theta_s = -90°$ to $\theta_s = 90°$; Polarization mode is vertical-to-vertical (VV) polarization. The simulation results are determined by one surface realization. Figure 2 shows the bi-static scattering coefficient of the PEC sphere and PEC rough surface based method of conventional MOM and FMM, where it can be seen that they are in good agreements. The corresponding numbers of the unknowns in target region and environment region are 5528 and 29833. In conventional MOM, the memory requirement and computation time are 3.93 GB and 1.03 h. However, in FMM, the memory is reduced to 2.34 GB, and the computation time only needs 0.24 h. The result shows the effectiveness and accuracy of FMM.

Secondly, for verify the hybrid SIE-KA-FMM method, consider an example of a combined conducting and dielectric sphere above Gauss rough surface. Working frequency is set as 1GHz; Size of environment is $L_x \times L_y$: $30\lambda \times 30\lambda$; Gauss rough surface is PEC surface; Here, statistic parameters of Gauss rough surface are: $h_{\mathrm{rms}} = 0.1\lambda$ and $l_{\mathrm{x}} = l_{\mathrm{y}} = 2.0\lambda$; The radius of combined sphere is 2.0λ; Combined sphere is comprised of a PEC hemisphere and a dielectric hemisphere with the permittivity $\varepsilon_{\mathrm{r}} = 4.0$; Height of combined sphere above the rough surface is 5.0λ; The incident angles are set as $\theta_i = 45°$ and $\varphi_i = 0°$; The observation angle

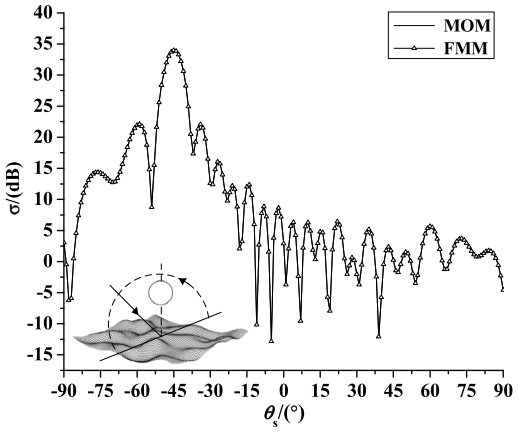

FIGURE 2. Compariso of bi-static scattering coefficient based on conventional MOM and FMM.

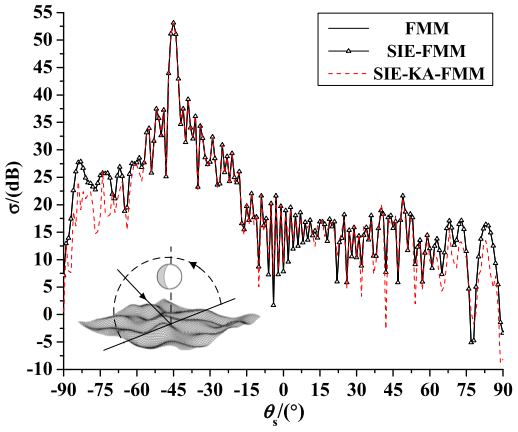

FIGURE 3. Compariso of bi-static scattering coefficient with different algorithm.

ranges from $\theta_s = -90°$ to $\theta_s = 90°$; Polarization mode is VV polarization. We choose two reference algorithms: FMM based on conventional coupled integral equation method and SIE-FMM to compare with the hybrid SIE-KA-FMM method in aspects of memory requirement and computation time. The bi-static scattering coefficient (BSC) of the composite scattering model is calculated by FMM, SIE-FMM and SIE-KA-FMM respectively. The simulation results are determined by one surface realization. In this paper, the computing platform is AMD processor of 2.3 GHz with 64 kernels and 64 GB RAM.

The corresponding numbers of the unknowns in target region and environment region are 43187 and 268497 by using FMM based on conventional coupled integral equation method. However, by introducing SIE, the number of unknowns for composite target reduces to 31228. As mentioned previously, by utilizing the hybrid SIE-KA method, the dimension of impedance matrix only depends on the number of target's unknowns rather that the total number, which will greatly reduce the memory requirement and computation time. The simulation results are shown in Figure.3. As we see, the simulation results by SIE-KA-FMM fairly well agree with FMM and SIE-FMM, meanwhile a discrepancy exists in the large scattering angle region. This inconsistency is unsurprising, primarily due to the fact that the KA method [30]–[32] has limitation in computing scattering from rough surface in the large scattering angle region. Table 1 gives the comparison of memory requirement and computation time of FMM, SIE-FMM and SIE-KA-FMM respectively. The memory requirement of SIE-KA-FMM is 24.43% of SIE-FMM, 17.65% of FMM. The consuming time of SIE-KA-FMM is 19.81% of SIE-FMM, 13.96% of FMM. The new hybrid method is efficient and accuracy for analyzing the electromagnetic scattering from combined conducting and dielectric target above rough surface.

Finally, we will give other two examples like composite cube and composite cylinder above Gauss rough surface, in order to verify the validation that this hybrid method can solve scattering problems of combined target for different

TABLE 1. Memory requirement and computation time of three solvers.

Solver	Memory Requirement(GB)	Computation time (h)
FMM	20.67	3.08
SIE-FMM	14.94	2.17
SIE-KA-FMM	3.65	0.43

shape. Working frequency is set as 1GHz. Concrete parameters of environment are the same as above example. Composite cube is comprised of a PEC cuboid and a dielectric cuboid with the permittivity $\varepsilon_r = (4.0, -j2.0)$ (which is the dark region in Figure 4). The side length of composite cube and its height above surface is 4.0λ and 5.0λ respectively. The cylinder is evenly divided into PEC part and dielectric part with the permittivity $\varepsilon_r = (4.0, -j2.0)$ (which is the dark region in Figure 5). The cylinder's height and radius of cylinder's bottom is 4.0λ and 2.0λ respectively. The height of cylinder above the surface is 5.0λ. The incident angles are set as $\theta_i = 45°$ and $\varphi_i = 0°$; The observation angle ranges from $\theta_s = -90°$ to $\theta_s = 90°$; Polarization mode is VV polarization. The results of them calculated respectively by FMM, SIE+FMM and SIE+KA+FMM are given in Figure 4 and Figure 5. As we see, the simulation results by SIE-KA-FMM fairly well agree with FMM and SIE-FMM, meanwhile a discrepancy exists in the large scattering angle region, and the reason causing this inconsistency is given in the computation example above.

III. NUMERICAL RESULTS AND ANALYSIS

In this section, the electromagnetic scattering characteristics of combined conducting and dielectric target above rough surface are analyzed by hybrid SIE-KA-FMM method. The differences of electromagnetic scattering from PEC target, dielectric target and composite target above rough surface are compared. The influences of permittivity of dielectric part, RMS and correlation length of rough surface, incident pitching or azimuth angle and target category on scattering characteristic are discussed.

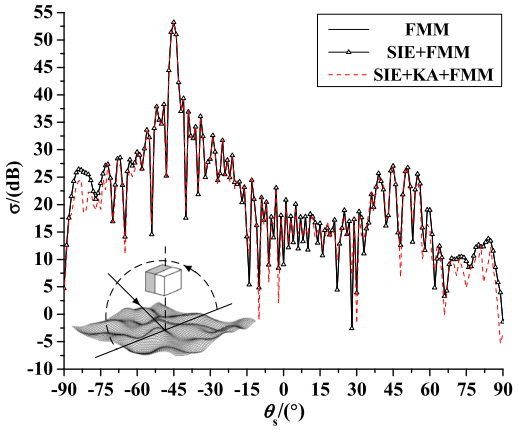

FIGURE 4. Comparison of bi-static scattering coefficient for composite cube above rough surface with different algorithm.

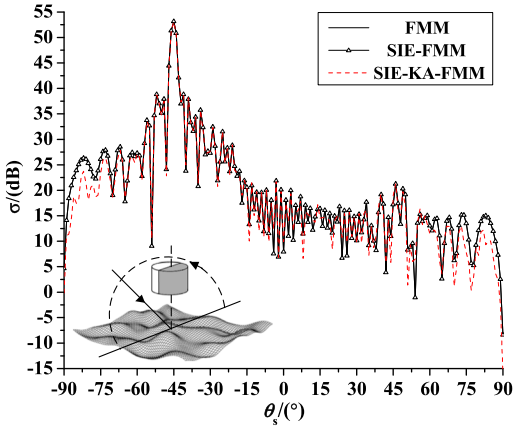

FIGURE 5. Comparison of bi-static scattering coefficient for composite cylinder above rough surface with different algorithm.

To begin with, we introduce the common simulation conditions of following computation examples: Working frequency is set as 1 GHz (except for example C); Polarization mode is VV polarization (except for example B). Rough surface model is generated by using Gauss spectral function, and the surface's material is PEC; The rough surface model is located in *xoy* plane and its size is $L_x \times L_y$: $30\lambda \times 30\lambda$; The height of target in following computation examples is set as 5λ. The following numerical simulations obtained by hybrid SIE-KA-FMM method are determined by averaging 30 Monte Carlo realizations.

A. INFLUENCE OF RELATIVE PERMITTIVITY ON SCATTERING CHARACTERISTIC

The effect of dielectric part in composite target is the core problem. Its electromagnetic attributions play a determinant role in scattering characteristic of target, which also has effect on the composite scattering in some degrees. The side length of composite cube is 4.0λ. As shown in Figure 6, composite cube is comprised of a PEC cuboid and a dielectric cuboid; Set the incident angle as: $\theta_i = 45°$, $\varphi_i = 0°$. The viewing angle θ_s is from $-90°$ to $90°$. Statistic parameters of Gauss rough surface are: $h_{\text{rms}} = 0.1\lambda$ and $l_{\text{x}} = l_{\text{y}} = 2.0\lambda$. The abbreviation Die1 and Die2 in Figure 6 presents relative permittivity $\varepsilon_{\text{r1}} = (4.0, -j2.0)$ and $\varepsilon_{\text{r2}} = (8.0, -j4.0)$ respectively. In Figure 6, the shadow part presents the dielectric region of composite target.

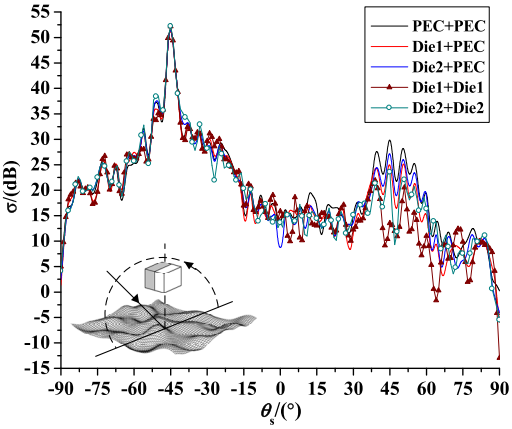

FIGURE 6. Bi-stati scattering coefficients with different combination of composite cube.

In Figure 6, there is an obvious peak value at the specular scattering position in every curve, and this peak value including its corresponding position would not vary with the change of target's property because the specular scattering characteristic of composite scattering mainly depends on the environment's properties. Due to the existence of cube, there is a strong backscattering existing near the scattering angle 45°. By comparison, the backscattering from pure PEC target above rough surface is the strongest. Correspondingly, the backscattering from pure dielectric target above rough surface is weak, and the pure dielectric target with smaller permittivity has weaker backscattering. Based on these two conclusions, comparing the curve of combination "Die1+PEC" and "Die2+PEC", an important can be obtained that the backscattering of combination "Die2+PEC" is stronger than "Die1+PEC", because composite target's dielectric part with bigger permittivity will cause stronger backscattering.

B. INFLUENCE OF POLARIZATION MODE ON SCATTERING CHARACTERISTIC

The selection of polarization mode has important effect on the scattering characteristic. The geometrical parameters of combined target are the same as computation example A. Set the permittivity of cube's dielectric part is $\varepsilon_{\text{r}} = (4.0, -j2.0)$. Set the incident angle as: $\theta_i = 45°$, $\varphi_i = 0°$. The viewing angle θ_s is from $-90°$ to $90°$. And the statistic parameters of rough surface are the same as computation example A.

In Figure 7, the bi-static scattering coefficient of cross-polarization is much smaller than that of co-polarization at all scattering angles. There is an obvious peak value at the specular scattering position in every polarization mode.

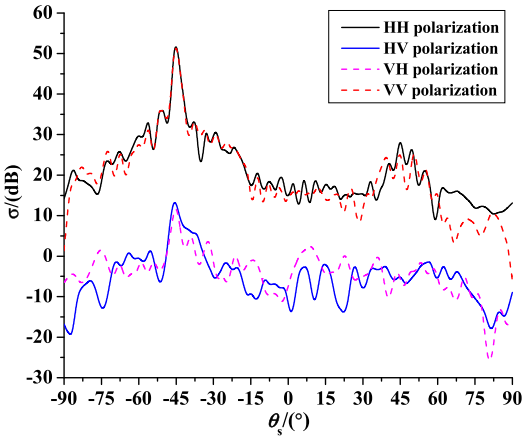

FIGURE 7. Bi-static scattering coefficients with different polarization mode.

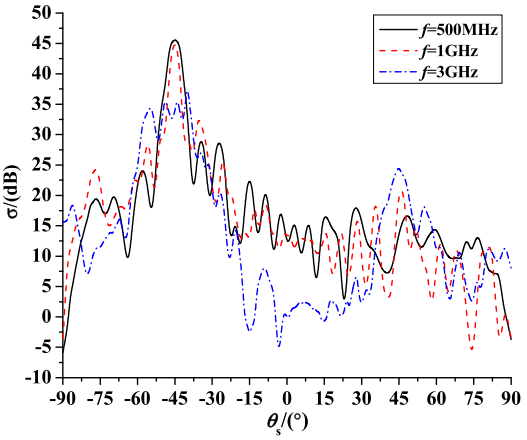

FIGURE 8. Bi-static scattering coefficients with different working frequency.

The curve trend of horizontal-to-horizontal (HH) mode is similar to VV mode, and the curve value of VV mode is smaller than HH mode at the scattering angle from 60° to 90°. In both HH and VV polarization mode, there is a strong backscattering existing near the scattering angle 45° due to the existence of cube, but in horizontal-to-vertical (HV) and vertical-to-horizontal (VH) polarization mode, the backscattering from target is not obvious.

C. INFLUENCE OF FREQUENCY ON SCATTERING CHARACTERISTIC

The EM scattering characteristics of combined cube above rough surface will be different when the working frequency is changed. Thus, we consider a smaller scattering model: Size of Gauss rough surface is $L_x \times L_y$: 6m × 6m; Statistic parameters of Gauss rough surface are: $h_{\rm rms} = 0.03$m and $l_{\rm x} = l_{\rm y} = 0.6$m; The side length of composite cube is 0.9m; The height of composite cube above the rough surface is 0.9m; Set the permittivity of cube's dielectric part is $\varepsilon_{\rm r} = (4.0, -j2.0)$. Set the incident angle as: $\theta_i = 45°$, $\varphi_i = 0°$. The viewing angle θ_s is from $-90°$ to 90°. Set the working frequency as: $f_1 = 500$MHz, $f_2 = 1.0$GHz and $f_3 = 3.0$GHz.

In Figure 8, with the increase of working frequency, the scattering energy near the specular scattering direction becomes dispersive. The reason causes this phenomenon is that the statistic parameters of rough surface are invariant with the increase of working frequency, but the relative roughness of rough surface will increase. On the other hand, with the increase of working frequency, the scattering energy of backscattering becomes stronger.

D. INFLUENCE OF ROUGH SURFACE'S STATISTIC PARAMETERS ON SCATTERING CHARACTERISTIC

The property of rough surface mainly depends on its statistic parameters. The geometrical parameters of combined target are the same as computation example A. Set the permittivity of cube's dielectric part is $\varepsilon_{\rm r} = (4.0, -j2.0)$. Set the incident angle as: $\theta_i = 45°$, $\varphi_i = 0°$. The viewing angle θ_s is from $-90°$ to 90°. The correlation length of rough surface is set as $l_{\rm x} = l_{\rm y} = 1.0\lambda$. The curves of composite scattering with different RMS $h_{\rm rms1} = 0.1\lambda$ and $h_{\rm rms2} = 0.3\lambda$ are given in Figure 9. As shown in Figure 9, with the increase of RMS, the peak value at the specular scattering direction disappears. Meanwhile, the backscattering becomes weaker than before. The reason causes the phenomenon is that the larger RMS determines rougher surface. The strong diffuse scattering characteristic makes the peak value disappear and the backscattering weaker.

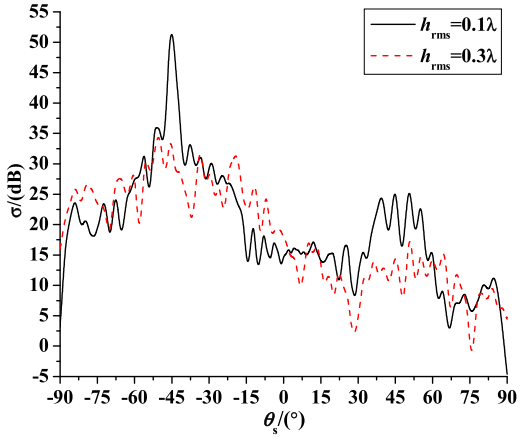

FIGURE 9. Bi-static scattering coefficients with different RMS.

Set the RMS as $h_{\rm rms} = 0.1\lambda$. The curves of composite scattering with different correlation length 2.0λ and 4.0λ are given. In Figure 10, with the increase of correlation length, the peak value at the specular scattering direction becomes bigger. Meanwhile, the backscattering becomes a little stronger than before. The reason causes the phenomenon is that the larger correlation length determines relatively flatter surface. Therefore, the specular scattering energy becomes more concentrated and the backscattering effect becomes stronger.

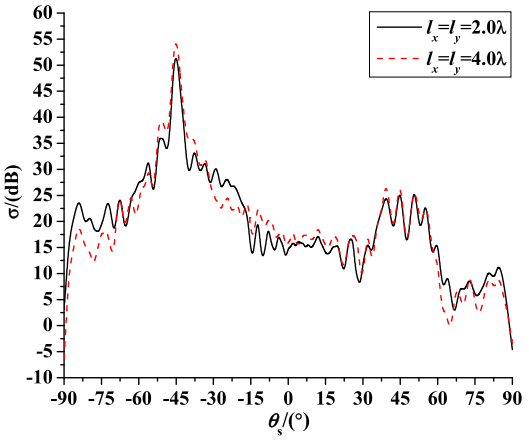

FIGURE 10. Bi-static scattering coefficients with different correlation length.

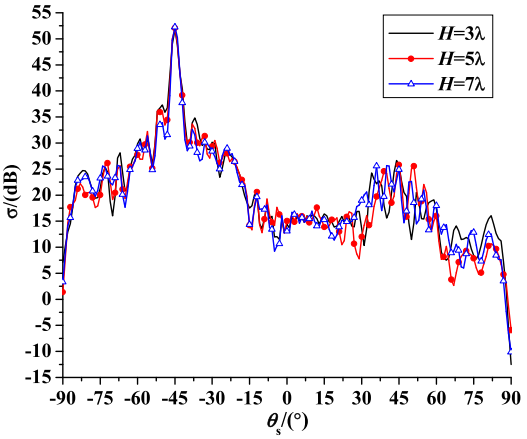

FIGURE 12. Bi-static scattering coefficients with different target's height.

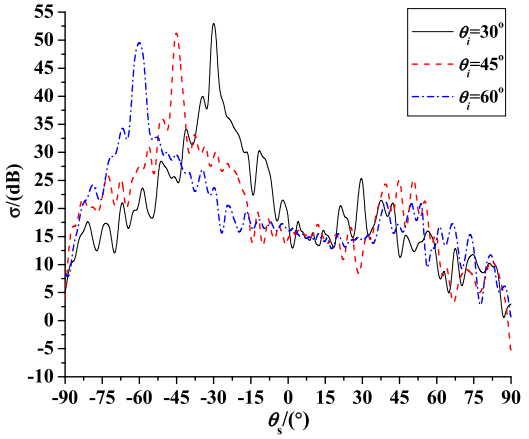

FIGURE 11. Bi-stati scattering coefficients with different incident angle.

E. INFLUENCE OF INCIDENT ANGLE ON SCATTERING CHARACTERISTIC

The geometrical and dielectric parameters of composite target are the same as computation example B. Statistic parameters of Gauss rough surface are: $h_{\rm rms} = 0.1\lambda$ and $l_{\rm x} = l_{\rm y} = 2.0\lambda$. (The rough surface's statistic parameters of following examples are the same as this computation example.) Set the incident angle as: $\theta_{i1} = 30°$, $\theta_{i2} = 45°$, $\theta_{i3} = 60°$. The viewing angle θ_s is from $-90°$ to $90°$. The composite target is the combination "Die1+PEC" in computation example A. In Figure 11, with the increase of incident angle, the peak value decreases and the corresponding angle position is moved with the incident angle. The backscattering with incident angle 45° is the most obvious among three curves.

F. INFLUENCE OF TARGET'S HEIGHT ON SCATTERING CHARACTERISTIC

The target's height will have effects on the mutual coupling between target and rough surface. The geometrical parameters of combined target are the same as computation example A. Set the permittivity of cube's dielectric part is $\varepsilon_{\rm r} = (4.0, -j2.0)$. Set the incident angle as: $\theta_i = 45°$, $\varphi_i = 0°$. The viewing angle θ_s is from $-90°$ to $90°$. And the statistic parameters of rough surface are the same as computation example A. Set the target's height as: $H_1 = 3\lambda$, $H_2 = 5\lambda$ and $H_3 = 7\lambda$.

In Figure 12, with the increase of target's height, the scattering coefficient near the specular direction decreases. This phenomenon indicates that if target is closer to the rough surface, the mutual effect between them is stronger which has more contributions to the specular scattering. By contrast, the change of target's height has weak effect on the backscattering, because the target and rough surface structure an analogous dihedral construction which will lead to strong backscattering even that target's height has been changed.

G. INFLUENCE OF TARGET'S CATEGORY ON SCATTERING CHARACTERISTIC

The target's shape and electromagnetic properties also plays a dominant role in its scattering characteristic. Firstly, we consider a composite cylinder with the radius and height of 2.0λ and 4.0λ, respectively. The cylinder is divided into four isopyknic parts which are separately marked as "1" to "4". Their corresponding positions are shown as in Figure 13. Set the incident angle as $\theta_i = 45°$. The viewing angle φ_s is from 0° to 360° and $\theta_s = 45°$. The abbreviation Die1 and Die2 in Figure 13 are the same in computation example A.

In Figure 13, the mono-static scattering energy from PEC target above rough surface distributes approximately well-proportioned in azimuth angle range. When the part 1 is altered to Die1, the value of mono-static scattering curve range from $\varphi_s = 0°$ to $\varphi_s = 90°$ dramatically decreases. When the part 2 is altered to Die1, the value of mono-static scattering curve range from $\varphi_s = 90°$ to $\varphi_s = 180°$ dramatically decreases. These two remarkable phenomena reflect that the dielectric part brings weaker backscattering than PEC part. Comparing the results of combination "Die1+Die1+PEC + PEC" and "Die2+Die2+PEC +PEC", a conclusion can be obtained: the dielectric part with bigger permittivity will

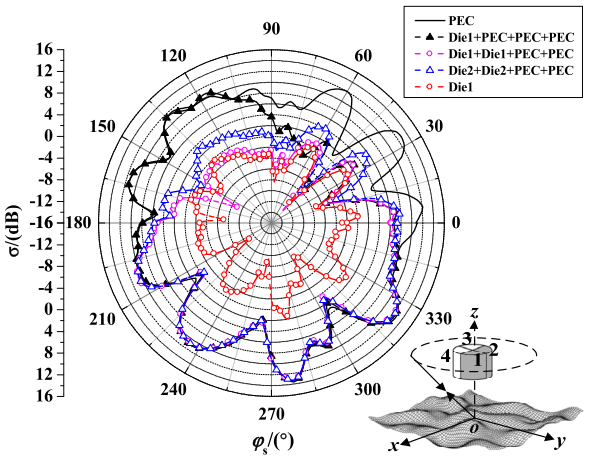

FIGURE 13. Mono-static scattering coefficients in azimuth distribution of composite cylinder above rough surface.

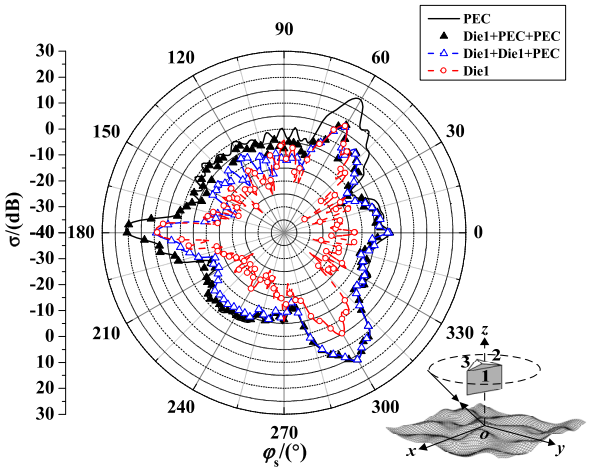

FIGURE 14. Mono-static scattering coefficients in azimuth distribution of composite triangular prism above rough surface.

cause stronger backscattering, which is accordance with the conclusion in computation example A. When the integrated material of target is altered to Die1, the mono-static scattering energy in all azimuth angle range dramatically decreases, which can also be an evidence of the above conclusion.

Secondly, we consider a composite triangular prism. The height of composite triangular prism is 4.0λ. Both top and bottom are equilateral triangle with side length of 4.0λ. The triangular prism is divided into three isopyknic parts which are separately marked as ''1'' to ''3''. Their corresponding positions are shown as in Figure 14. Set the incident angle as $\theta_i = 45°$. The viewing angle $\varphi_s$is from 0° to 360° and θ_s =45°. The abbreviation Die1 and Die2 in Figure 14 are the same in computation example A.

In Figure 14, due to the triangular prism's special structure, the vertical line of three sides are along the 60°, 180° and 300°, thus, we can easily observe that there are three strong peaks existing near the azimuth angle 60°, 180° and 300° respectively when the scattering comes from pure PEC target above rough surface. When the part 1 is altered to Die1, the value of mono-static scattering curve range from $\varphi_s = 0°$ to $\varphi_s = 120°$ decreases, among these angles the decrease of value near the $\varphi_s = 60°$ is remarkable. When the part 2 is altered to Die1, the value of mono-static scattering curve range from $\varphi_s = 120°$ to $\varphi_s = 240°$ also decreases, among these angles the decrease of value near the $\varphi_s = 180°$ is remarkable. The result verifies that it is not the unique phenomenon existing in composite cylinder which contains curved surface structure. Compared to the results of computation example D, the composite triangular prism containing plane structure has the similar conclusion: the dielectric part brings weaker backscattering than PEC part. When the integrated material of target is altered to Die1, the mono-static scattering energy in all azimuth angle range decreases.

H. A COMPOSITE MISSILE MODEL

We build a composite missile model illustrated in Figure 15, which includes its concrete geometrical parameters. The working frequency is 1 GHz. The head of composite missile model is toward the positive direction of x-axis. The nose of the missile consists of dielectric material with permittivity $\varepsilon_r = (4.0, -j2.0)$ which is marked as Die1. Set the incident angle as $\theta_i = 45°$. The viewing angle φ_s is from 0° to 360° and $\theta_s = 45°$. Firstly, we have to explain the legends in Figure 16 orderly: ''Com+Sur'' denotes scattering from composite missile above rough surface; ''PEC+Sur'' denotes scattering from pure PEC missile above rough surface; ''Sur'' denotes scattering from rough surface; ''Die1+PEC'' denotes scattering from composite missile consisting of dielectric part with permittivity Die1 and PEC part; ''PEC'' denotes scattering from pure PEC missile.

As shown in Figure 16, in the curve of Mono-static scattering coefficients of composite missile and rough surface, there is an obvious peak value existing at scattering angle $\theta_s = 0°$ because almost of scattering energy comes from rough surface when illuminated vertically. Comparing with the curve of combination ''PEC+Sur'', we can find that the change of nose's material does not have the dominant effect on the total field. Both of the curves of combination ''Com+Sur'' and ''PEC+Sur'' are similar to the curve of scattering from pure surface, and only a little difference existing at some scattering angles. Therefore, a further comparison is made to express some detailed phenomena.

As shown in Figure 16, when the nose's material of target is altered to Die1, there are two phenomena that deserve our attention: firstly, the backscattering from composite missile becomes weaker than pure PEC missile in the angle range of $-76° \sim -68°$, $-66° \sim -61°$, $-58° \sim -49°$ and $7° \sim 27°$; secondly, its backscattering from nose core direction (when $\theta_s = 90°$) is weaker than pure PEC target about 5.451dB. The result demonstrates the conclusion that the dielectric structure would decrease the energy of backscattering, which is widely

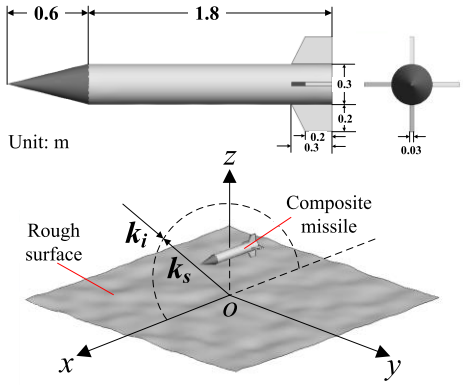

FIGURE 15. Geometrical parameters and position information of composite missile model.

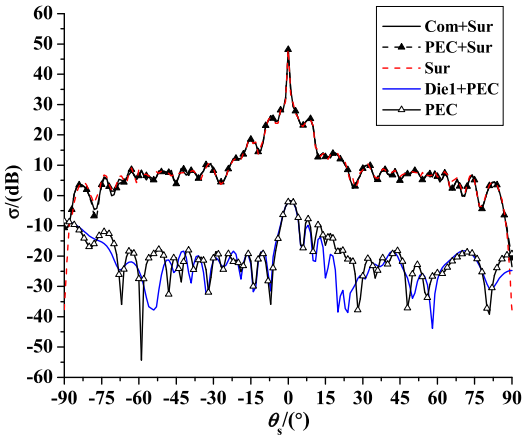

FIGURE 16. Mono-static scattering coefficients of composite missile and rough surface.

applied in the field of stealth technology for cruise missile or fighter plane.

IV. CONCLUSION

In this paper, an efficient hybrid SIE-KA-FMM method is developed for analyzing the electromagnetic scattering from combined conducting and dielectric objects above rough surface. Several numerical results are presented to demonstrate the computation efficiency and precision of the hybrid method. The differences of electromagnetic scattering from PEC target, dielectric target and composite target above rough surface are compared. Moreover, the influences of permittivity of dielectric part, polarization mode, working frequency, root mean square (RMS) and correlation length of rough surface, incident pitching or azimuth angle, target height and target category on scattering characteristic are discussed. Consequently, the proposed hybrid SIE-KA-FMM method can be used as an efficient tool to solve the practical electromagnetic scattering about combined conducting and dielectric objects in the real environment, during radar detection remote sensing and stealth technology etc.. The further work of our research group will focus on the scattering problems about combined conducting and dielectric objects above dielectric rough surface or layered surface, in order to make the conclusions close to practical natural situations.

APPENDIX

$$U_{im}^{\mathrm{D}44} = M_{im}^{\mathrm{D}44} = -\frac{k_0^2}{16\pi^2}\int_{\Gamma_{4i}} e^{-jk_0\hat{\mathbf{k}}\cdot\mathbf{r}_{im}}(\bar{\bar{\mathbf{I}}} - \hat{\mathbf{k}}\hat{\mathbf{k}})\mathbf{f}_{4i}\times\hat{\mathbf{k}}_i dS \tag{36}$$

$$V_{jm'}^{\mathrm{D}qq} = \int_{\Gamma_{qj}} e^{jk_0\hat{\mathbf{k}}\cdot\mathbf{r}_{jm'}}(\mathbf{f}_{qj}(\mathbf{r}_{jm'})\cdot\hat{\mathbf{e}}_{i\parallel}\hat{\mathbf{e}}_{i\parallel} + \mathbf{f}_{qj}(\mathbf{r}_{jm'})\cdot\hat{\mathbf{e}}_{i\perp}\hat{\mathbf{e}}_{i\perp})dS' \quad q = 1, 2. \tag{37}$$

$$N_{jm'}^{\mathrm{D}qq} = \int_{\Gamma_{qj}} e^{jk_0\hat{\mathbf{k}}\cdot\mathbf{r}_{jm'}} \times(\Gamma_{\parallel}\mathbf{f}_{qj}(\mathbf{r}_{jm'})\cdot\hat{\mathbf{e}}_{i\parallel}\hat{\mathbf{e}}_{i\parallel} + \Gamma_{\perp}\mathbf{f}_{qj}(\mathbf{r}_{jm'})\cdot\hat{\mathbf{e}}_{i\perp}\hat{\mathbf{e}}_{i\perp})dS' \quad q = 1, 2. \tag{38}$$

$$U_{im}^{\mathrm{F}44} = M_{im}^{\mathrm{F}44} = -\frac{k_0^2}{16\pi^2}\int_{\Gamma_{4i}} e^{-jk_0\hat{\mathbf{k}}\cdot\mathbf{r}_{im}}\mathbf{f}_{4i}\times\hat{\mathbf{k}}_i dS \tag{39}$$

$$V_{jm'}^{\mathrm{F}22} = \int_{\Gamma_{2j}} e^{jk_0\hat{\mathbf{k}}\cdot\mathbf{r}_{jm'}}(\mathbf{f}_{2j}(\mathbf{r}_{jm'})\times\hat{\mathbf{k}}\cdot\hat{\mathbf{e}}_{i\parallel}\hat{\mathbf{e}}_{i\parallel} + \mathbf{f}_{2j}(\mathbf{r}_{jm'}) \times\hat{\mathbf{k}}\cdot\hat{\mathbf{e}}_{i\perp}\hat{\mathbf{e}}_{i\perp})dS' \tag{40}$$

$$N_{jm'}^{\mathrm{F}22} = \int_{\Gamma_{2j}} e^{jk_0\hat{\mathbf{k}}\cdot\mathbf{r}_{jm'}}(\Gamma_{\parallel}\mathbf{f}_{2j}(\mathbf{r}_{jm'})\times\hat{\mathbf{k}}\cdot\hat{\mathbf{e}}_{i\parallel}\hat{\mathbf{e}}_{i\parallel} + \Gamma_{\perp}\mathbf{f}_{2j}(\mathbf{r}_{jm'}) \times\hat{\mathbf{k}}\cdot\hat{\mathbf{e}}_{i\perp}\hat{\mathbf{e}}_{i\perp})dS' \tag{41}$$

$$U_{im}^{\mathrm{Q}pp} = \frac{k_0^2}{16\pi^2}\int_{\Gamma_{pi}} e^{-jk_0\hat{\mathbf{k}}\cdot\mathbf{r}_{im}}\mathbf{f}_{pi}(\mathbf{r}_{im})\cdot(\bar{\bar{\mathbf{I}}} - \hat{\mathbf{k}}\hat{\mathbf{k}})dS, \quad p = 1, 2. \tag{42}$$

$$V_{jm'}^{\mathrm{Q}qq} = \int_{\Gamma_{qj}} e^{jk_0\hat{\mathbf{k}}\cdot\mathbf{r}_{jm'}}\mathbf{f}_{qj}(\mathbf{r}_{jm'})dS', \quad q = 1, 2. \tag{43}$$

$$U_{im}^{\mathrm{P}pp} = \frac{k_0^2}{16\pi^2}\int_{\Gamma_{pi}} e^{-jk_0\hat{\mathbf{k}}\cdot\mathbf{r}_{im}}(\hat{\mathbf{k}}\times\mathbf{f}_{pi})dS, \quad p = 1, 2. \tag{44}$$

$$V_{jm'}^{\mathrm{P}22} = \int_{\Gamma_{2j}} e^{jk_0\hat{\mathbf{k}}\cdot\mathbf{r}_{jm'}}\mathbf{f}_{2j}(\mathbf{r}_{jm'})dS' \tag{45}$$

$$U_{im}^{\mathrm{R}pp} = \frac{k_0^2}{16\pi^2}\int_{\Gamma_{pi}} e^{-jk_0\hat{\mathbf{k}}\cdot\mathbf{r}_{im}}\mathbf{f}_{pi}(\mathbf{r}_{im})\cdot(\bar{\bar{\mathbf{I}}} - \hat{\mathbf{k}}\hat{\mathbf{k}})dS, \quad p = 1, 2. \tag{46}$$

$$V_{jm'}^{\mathrm{R}44} = \int_{\Gamma_{4j}} e^{jk_0\hat{\mathbf{k}}\cdot\mathbf{r}_{jm'}}\mathbf{f}_{4j}(\mathbf{r}_{jm'})dS' \tag{47}$$

$$U_{im}^{\tilde{M}22} = -\frac{1}{l_{2i}}\cdot\frac{k_1^2}{16\pi^2}\int_{l_{2i}} e^{-jk_1\hat{\mathbf{k}}\cdot\mathbf{r}_{im}}(\hat{\mathbf{k}}\times\hat{l}_{2i})dl \tag{48}$$

$$V_{jm'}^{\tilde{M}qq} = \int_{\Gamma_{d(Sq)j}} e^{jk_1\hat{\mathbf{k}}\cdot\mathbf{r}_{jm'}}f_{qj}(\mathbf{r}_{jm'})dS', \quad q = 2, 3. \tag{49}$$

$$U_{im}^{\tilde{N}22} = \frac{1}{l_{2i}}\cdot\frac{\eta_1}{\eta_0}\cdot\frac{k_1^2}{16\pi^2}\int_{l_{2i}} e^{-jk_1\hat{\mathbf{k}}\cdot\mathbf{r}_{im}}\hat{l}_{2i}\cdot(\bar{\bar{\mathbf{I}}} - \hat{\mathbf{k}}\hat{\mathbf{k}})dl \tag{50}$$

$$V_{jm'}^{\tilde{N}qq} = \int_{\Gamma_{d(Sq)j}} e^{jk_1\hat{\mathbf{k}}\cdot\mathbf{r}_{jm'}}f_{qj}(\mathbf{r}_{jm'})dS', \quad q = 2, 3. \tag{51}$$

$$U_{im}^{\tilde{B}33} = \frac{\eta_1}{\eta_0}\cdot\frac{k_1^2}{16\pi^2}\int_{T_{3i}} e^{-jk_1\hat{\mathbf{k}}\cdot\mathbf{r}_{im}}f_{3i}(\mathbf{r}_{im})\cdot(\bar{\bar{\mathbf{I}}} - \hat{\mathbf{k}}\hat{\mathbf{k}})dS \tag{52}$$

$$V_{jm'}^{\tilde{B}qq} = \int_{\Gamma_{d(Sq)j}} e^{jk_1\hat{\mathbf{k}}\cdot\mathbf{r}_{jm'}}f_{qj}(\mathbf{r}_{jm'})dS', \quad q = 2, 3. \tag{53}$$

REFERENCES

[1] S. M. Rao, C.-C. Cha, R. L. Cravey, and D. L. Wilkes, "Electromagnetic scattering from arbitrary shaped conducting bodies coated with lossy materials of arbitrary thickness," *IEEE Trans. Antennas Propag.*, vol. 39, no. 5, pp. 627–631, May 1991.

[2] Y.-W. Wei, L.-X. Guo, A.-Q. Wang, and Z.-S. Wu, "Application of multiregion model to EM scattering from a dielectric rough surface with or without a target above it," *IEEE Trans. Antennas Propag.*, vol. 61, no. 11, pp. 5607–5620, Nov. 2013.

[3] T. K. Sarkar and E. Arvas, "An integral equation approach to the analysis of finite microstrip antennas: Volume/surface formulation," *IEEE Trans. Antennas Propag.*, vol. 38, no. 3, pp. 305–312, Mar. 1990.

[4] S. M. Rao, T. K. Sarkar, P. Midya, and A. R. Djordevic, "Electromagnetic radiation and scattering from finite conducting and dielectric structures: Surface/surface formulation," *IEEE Trans. Antennas Propag.*, vol. 39, no. 7, pp. 1034–1037, Jul. 1991.

[5] C. C. Lu and W. C. Chew, "A coupled surface-volume integral equation approach for the calculation of electromagnetic scattering from composite metallic and material targets," *IEEE Trans. Antennas Propag.*, vol. 48, no. 12, pp. 1866–1868, Dec. 2000.

[6] H. Huang, L. Tsang, E. G. Njoku, A. Colliander, T.-H. Liao, and K.-H. Ding, "Propagation and scattering by a layer of randomly distributed dielectric cylinders using Monte Carlo simulations of 3D Maxwell equations with applications in microwave interactions with vegetation," *IEEE Access*, vol. 5, pp. 11985–12003, 2017.

[7] K. S. Yee, J. ShuanChen, and A. H. Chang, "Conformal finite-different time-domain (FDTD) with overlapping grids," *IEEE Trans. Antennas Propag.*, vol. 40, no. 9, pp. 1068–1075, Sep. 1992.

[8] C. M. Furse, S. P. Mathur, and O. P. Gandhi, "Improvements to the finite-difference time-domain method for calculating the radar cross section of a perfectly conducting target," *IEEE Trans. Microw. Theory Techn.*, vol. 38, no. 7, pp. 919–927, Jul. 1990.

[9] P. Liu and Y.-Q. Jin, "The finite-element method with domain decomposition for electromagnetic bistatic scattering from the comprehensive model of a ship on and a target above a large-scale rough sea surface," *IEEE Trans. Geosci. Remote Sens.*, vol. 42, no. 5, pp. 950–956, May 2004.

[10] P. Paul and J. P. Webb, "Reducing computational costs using a multi-region finite element method for electromagnetic scattering," *IET Microw., Antennas Propag.*, vol. 2, no. 5, pp. 427–433, Aug. 2008.

[11] S. M. Rao, D. R. Wilton, and A. W. Glisson, "Electromagnetic scattering by surfaces of arbitrary shape," *IEEE Trans. Antennas Propag.*, vol. AP-30, no. 3, pp. 409–418, May 1982.

[12] J. He, T. Yu, N. Geng, and L. Carin, "Method of moments analysis of electromagnetic scattering from a general three-dimensional dielectric target embedded in a multilayered medium," *Radio Sci.*, vol. 35, no. 2, pp. 305–313, 2016.

[13] K. C. Donepudi, J.-M. Jin, and W. C. Chew, "A higher order multilevel fast multipole algorithm for scattering from mixed conducting/dielectric bodies," *IEEE Trans. Antennas Propag.*, vol. 51, no. 10, pp. 2814–2821, Oct. 2003.

[14] W. B. Ewe, L. W. Li, and M. S. Leong, "Solving mixed dielectric/conducting scattering problem using adaptive integral method," *Prog. Electromagn. Res.*, vol. 46, pp. 143–163, 2004.

[15] H. Gan and W. C. Chew, "A discrete BCG-FFT algorithm for solving 3D inhomogeneous scatterer problems," *J. Electromagn. Waves Appl.*, vol. 9, no. 10, pp. 1339–1357, 1995.

[16] J. M. Song and W. C. Chew, "Multilevel fast-multipole algorithm for solving combined field integral equations of electromagnetic scattering," *Microw. Opt. Technol. Lett.*, vol. 10, no. 1, pp. 14–19, Sep. 1995.

[17] V. V. S. Prakash and R. Mittra, "Characteristic basis function method: A new technique for efficient solution of method of moments matrix equations," *Microw. Opt. Technol. Lett.*, vol. 36, pp. 95–100, Jan. 2003.

[18] Y. L. Xu, H. Yang, and W. K. Yu, "Scattering analysis of periodic composite metallic and dielectric structures with synthetic basis functions," *Appl. Comput. Electromagn. Soc. J.*, vol. 30, no. 10, pp. 1059–1067, 2015.

[19] Y. Xu, H. Yang, W. Yu, X. Liu, and R. Shen, "Scattering analysis of nonperiodic composite metallic and dielectric structures using synthetic functions," *IEEE Antennas Wireless Propag. Lett.*, vol. 16, pp. 3079–3083, 2017.

[20] Y. Xu, H. Yang, J. Lu, W. Yu, W. Yin, and D. Peng, "Improved synthetic basis functions method for nonperiodic scaling structures with arbitrary spatial attitudes," *IEEE Trans. Antennas Propag.*, vol. 65, no. 9, pp. 4728–4741, Sep. 2017.

[21] A. J. Poggio and E. K. Miller, "Integral equation solutions of three-dimensional scattering problems," *Comput. Techn. Electromagn.*, vol. 4, pp. 159–264, 1973.

[22] T.-K. Wu and L. L. Tsai, "Scattering from arbitrarily-shaped lossy dielectric bodies of revolution," *Radio Sci.*, vol. 12, no. 5, pp. 709–718, Sep./Oct. 1977.

[23] R. F. Harrington, "Boundary integral formulations for homogeneous material bodies," *J. Electromagn. Waves Appl.*, vol. 3, no. 1, pp. 1–15, 1989.

[24] M. S. Yeung, "Single integral equation for electromagnetic scattering by three-dimensional homogeneous dielectric objects," *IEEE Trans. Antennas Propag.*, vol. 47, no. 10, pp. 1615–1622, Oct. 1999.

[25] P. Wang, M. Xia, and L. Zhou, "Analysis of scattering by combined conducting and dielectric bodies using single integral equation method and fast multipole method," in *Proc. Asia–Pacific Microw. Conf. Proc.*, vol. 5, Dec. 2005, p. 4.

[26] P. Wang, M. Y. Xia, and L. Z. Zhou, "Analysis of scattering by composite conducting and dielectric bodies using the single integral equation method and multilevel fast multipole algorithm," *Microw. Opt. Technol. Lett.*, vol. 48, no. 6, pp. 1055–1059, 2006.

[27] G. X. Zou, C. M. Tong, H. L. Sun, T. Wang, and P. Peng, "A hybrid method for electromagnetic scattering from target above composite rough surface of ground and near sea in adjacent region," *Electromagnetics*, vol. 38, no. 7, pp. 415–437, 2018.

[28] N. Bi, J. Qin, and T. Jiang, "Partition detection and location of a Kelvin wake on a 2-D rough sea surface by feature selective validation," *IEEE Access*, vol. 6, pp. 16345–16352, 2018.

[29] G. Zilman, A. Zapolski, and M. Marom, "On detectability of a ship's Kelvin wake in simulated SAR images of rough sea surface," *IEEE Trans. Geosci. Remote Sens.*, vol. 53, no. 2, pp. 609–619, Jun. 2014.

[30] R. Wang, G. Li-Xin, M. Jun, and W. Zhen-Sen, "Hybrid method for investigation of electromagnetic scattering from conducting target above the randomly rough surface," *Chin. Phys. B*, vol. 18, no. 4, pp. 1503–1511, 2009.

[31] S. Y. He and G. Q. Zhu, "A hybrid MM-PO method combining UV technique for scattering from two-dimensional target above a rough surface," *Microw. Opt. Technol. Lett.*, vol. 49, no. 12, pp. 2957–2960, 2010.

[32] J. Li, L. X. Guo, and Q. He, "Hybrid FE-BI-KA method in analysing scattering from dielectric object above sea surface," *Electron. Lett.*, vol. 47, no. 20, pp. 1147–1148, 2011.

[33] G. S. Brown, "Backscattering from a Gaussian-distributed perfectly conducting rough surface," *IEEE Trans. Antennas Propag.*, vol. AP-26, no. 3, pp. 472–482, May 1978.

[34] Y.-Z. J. Wang, R. Ananth, and P. A. Tatem, "Numerical simulation of solid combustion with a robust conjugate gradient solution for pressure," Naval Res. Lab., Washington, DC, USA, Jul. 2002, pp. 10–13.

[35] S. Yan, J. M. Jin, and Z. P. Nie, "A comparative study of Calderón preconditioners for PMCHWT equations," *IEEE Trans. Antennas Propag.*, vol. 58, no. 7, pp. 2375–2383, Jul. 2010.

[36] N. V. Budko and A. B. Samokhin, "Spectrum of the volume integral operator of electromagnetic scattering," *SIMA J. Sci. Comput.*, vol. 28, no. 2, pp. 682–700, 2005.

[37] H. X. Ye and Y. Q. Jin, "Parameterization of tapered incident wave for electromagnetic scattering simulation from randomly rough surface," *IEEE Trans. Antennas Propag.*, vol. 53, no. 3, pp. 1234–1237, Mar. 2005.

[38] H. L. Sun, C. M. Tong, and G. X. Zou, "High efficiency iterative solver for modeling composite rough surface electromagnetic scattering," *Electromagnetics*, vol. 37, no. 2, pp. 113–126, 2017.

GAOXIANG ZOU was born in Hunan, China, in 1993. He received the B.S. degree in radar engineering, in 2015, and the M.S. degree in electronics science and technology, in 2018, from Air Force Engineering University, Xi'an, China, where he is currently pursuing the Ph.D. degree in electromagnetic theory and engineering. His research interests include computational electromagnetism, Brewster effect, multipath effect, modeling theory of divisional environments, and the electromagnetic scattering characteristics of composite targets above divisional environments.

CHUANGMING TONG was born in Hubei, China, in 1964. He received the M.S. and Ph.D. degrees in electromagnetic field and microwave technology from the Air Force Missile College, in 1988 and 1999, respectively. From 1999 to 2002, he was a Visiting Scholar with the State Key Laboratory of Millimeter Waves, Southeast University, Nanjing, China. He is currently a Professor and a Doctoral Supervisor with the Air and Missile Defense College, Air Force Engineering University. He is also the Chief Scientist of the National 973 project. His research interests include microwave remote sensing, computational electromagnetism, polarimetric and interferometric applications of microwave data, numerical modeling, and ground penetrating radar, through wall imaging and stealth technology. He has received various fellowships and awards from national and international bodies.

HUALONG SUN was born in Shaanxi, China, in 1982. He received the B.S. degree in information engineering from the Nanjing University of Aeronautics and Astronautics, Nanjing, China, in 2004, the M.S. degree in electromagnetic field and microwave technology from Southeast University, Nanjing, in 2007, and the Ph.D. degree in electromagnetic theory and engineering from the Air and Missile Defense College, Air Force Engineering University, Xi'an, China, in 2017, where he is currently a Postdoctoral Student in electronics science and technology. His research interests include multipath effect, radar signal processing, fast electromagnetic calculation method, and electromagnetic scattering characteristics of complex targets and complicated circumstances.

PENG PENG was born in Jiangxi, China, in 1990. He received the B.S. degree in radar engineering and the M.S. degree in electromagnetic field and microwave technology from Air force Engineering University, in 2011 and 2013, respectively. From 2014 to 2015, he took the Initial Officer Training Course (IOTC) in the Royal Air force College Cranwell, U.K. He is currently pursuing the Ph.D. degree with the School of Physics and Optoelectronic Engineering, Xidian University, Xi'an, China. His research interests include fast algorithms for computational electromagnetics, radar scattering characteristics of the complex target and environment surface, and radar imaging.

TAO SONG was born in Shandong, China, in 1990. He received the B.S. degree in electromagnetic wave propagation and antenna, in 2013, and the M.S degree in electromagnetic field and microwave technology, in 2016, from Air Force Engineering University, Xi'an, China, where he is currently pursuing the Ph.D. degree in electronics science and technology. His research interests include computational electromagnetics and wave scattering from rough surface.